



# Mixed-mode $J$ -integral formulation and implementation using graded elements for fracture analysis of nonhomogeneous orthotropic materials

Jeong-Ho Kim, Glaucio H. Paulino \*

*Department of Civil and Environmental Engineering, University of Illinois at Urbana-Champaign, Newmark Laboratory,  
205 North Mathews Avenue, Urbana, IL 61801, USA*

Received 30 October 2001; received in revised form 1 April 2002

## Abstract

The path-independent  $J_k^*$ -integral, in conjunction with the finite element method (FEM), is presented for mode I and mixed-mode crack problems in orthotropic functionally graded materials (FGMs) considering plane elasticity. A general procedure is presented where the crack is arbitrarily oriented, i.e. it does not need to be aligned with the principal orthotropy directions. Smooth spatial variations of the independent engineering material properties are incorporated into the element stiffness matrix using a “generalized isoparametric formulation”, which is natural to the FEM. Both exponential and linear variations of the material properties are considered. Stress intensity factors and energy release rates for pure mode I and mixed-mode boundary value problems are numerically evaluated by means of the equivalent domain integral especially tailored for orthotropic FGMs. Numerical results are discussed and validated against available theoretical and numerical solutions.

© 2002 Elsevier Science Ltd. All rights reserved.

*Keywords:* Functionally graded material; Orthotropic material; Stress intensity factor; Finite element method; Equivalent domain integral;  $J_k^*$ -integral

## 1. Introduction

Functionally graded materials (FGMs) possess a continuous spatial distribution of the volume fractions of two or more basic materials. These materials were initially introduced to take advantage of different properties of its constituents, e.g. heat and corrosion resistance of ceramics together

with mechanical strength and toughness of metals. With such materials, it is possible to improve thermal or mechanical stress relaxation (Choules and Kokini, 1993; Lee and Erdogan, 1995), and to increase bonding strength and toughness (Kurihara et al., 1990) along coating/substrate interfaces. Investigations on FGMs have found various applications (Koizumi, 1993; Hirai, 1993; Suresh and Mortensen, 1998), which include high temperature (Igari et al., 1990); electronics and magnetics (Tani and Liu, 1993; Hirano et al., 1993; Osaka et al., 1990; Watanabe et al., 1993); optics (Koike, 1992);

\* Corresponding author. Tel.: +1-217-333-3817; fax: +1-217-265-8041.

E-mail address: [paulino@uiuc.edu](mailto:paulino@uiuc.edu) (G.H. Paulino).

thermionics (Desplat, 1996); biomaterials (Watari et al., 1996; Oonishi et al., 1994); and so on. A description of design, modeling, processing, and evaluation of FGMs, as well as their applications, can be found in the books by Suresh and Mortensen (1998) and by Miyamoto et al. (1999), and also in the review article by Paulino et al. (2003).

Extensive studies have been carried out on fracture mechanics under mechanical (Delale and Erdogan, 1983; Erdogan and Wu, 1993; Ozturk and Erdogan, 1997, 1999) or thermal (Noda and Jin, 1993; Jin and Noda, 1993; Erdogan and Wu, 1996; Jin and Batra, 1996; Jin and Paulino, 2001) loading in FGMs. Eischen (1987) has investigated the  $J_k^*$ -integral in the form of line integral for mixed-mode cracks in nonhomogeneous materials using the finite element method (FEM). Honein and Herrmann (1997) have studied the path-independent  $J$ -integral based on conservation laws for elastic nonhomogeneous materials. Gu et al. (1999) have proposed a simplified method based on the standard  $J$ -integral (Rice, 1968) to evaluate SIFs in FGMs using the equivalent domain integral (EDI) technique. They considered material properties at the Gauss integration points and selected very small domains to avoid the effect of the extra term in the domain integral due to nonhomogeneity. Other authors have used the interaction integral method to compute SIFs in FGMs (Dolbow and Gosz, 2002; Rao and Rahman, in press; Kim and Paulino, submitted for publication). Anlas et al. (2000) have evaluated SIFs in FGMs by the FEM where the material property variation was discretized by assigning different homogeneous elastic properties to each element. Chen et al. (2000) have presented a modified  $J$ -integral for FGMs using the element-free Galerkin method. Gu et al. (1999), Anlas et al. (2000), and Chen et al. (2000) have considered a pure mode I crack where the crack is parallel to the material gradation. Marur and Tippur (2000) have considered a crack normal to the elastic gradient and have performed FEM analysis along with experiments. In the particular case of Marur and Tippur (2000), no extra term (due to material nonhomogeneity) arises in the  $J$ -integral. Bao and Wang (1995) have studied multiple cracking in functionally graded ceramic/metal coatings using the FEM. Bao and Cai (1997) have investi-

gated delamination cracking and buckling in a functionally graded ceramic/metal substrate under mechanical and thermal loads using the FEM.

All the investigations cited above have been done for isotropic FGMs and no consideration of orthotropy has been made. In general, the manufacturing of ceramic-metal FGMs requires sophisticated processing techniques, and the nature of processing techniques may cause the FGMs to lose isotropy. For instance, graded materials processed by a plasma spray technique generally have a lamellar structure (Sampath et al., 1995), whereas the materials processed by electron beam physical vapor deposition technique have a columnar structure (Kaysner and Ilschner, 1995). In such cases, we can assume that the graded material is not isotropic but orthotropic. Previous work on modeling of fracture in orthotropic FGMs include those by Gu and Asaro (1997), who performed theoretical studies in a four point bending specimen; and by Ozturk and Erdogan (1997, 1999), who investigated mode I and mixed mode crack problems in an infinite medium using integral equations. In this paper, extension of the path-independent  $J_k^*$ -integral methodology for isotropic FGMs is made to orthotropic FGMs (Eischen, 1987; Kim and Paulino, 2002a). To discretize the variation of the orthotropic material properties, the “generalized isoparametric formulation” (GIF) is used to formulate the stiffness matrix in the FEM (Kim and Paulino, 2002a,b).

The organization of this paper is as follows. Section 2 discusses crack-tip fields in two-dimensional orthotropic FGMs. Section 3 presents the domain-independent  $J_k^*$ -integral formulation in orthotropic FGMs, which includes the nonlinear relations between  $J_k^*$  ( $k = 1, 2$ ) and the modes I and II stress intensity factors (SIFs). Section 4 contains the finite element implementation. Section 5 includes numerical examples evaluated by means of the  $J_k^*$  integral. Finally, Section 6 presents some final remarks and concludes this investigation.

## 2. Crack-tip fields in orthotropic FGMs

The linear elastic stress–strain relations are given by

$$\varepsilon_{ij} = S_{ijkl}\sigma_{kl} \quad (i, j, k, l = 1, 2, 3) \quad (1)$$

where  $\sigma_{ij}$  is the linear stress tensor,  $\varepsilon_{ij}$  is the linear strain tensor, and  $S_{ijkl}$  is the fourth-order compliance tensor. A contracted notation  $a_{ij}$  is introduced for  $S_{ijkl}$  as follows (Lekhnitskii, 1968):

$$\varepsilon_i = a_{ij}\sigma_j, \quad a_{ij} = a_{ji} \quad (i, j = 1, 2, \dots, 6) \quad (2)$$

where the compliance coefficients,  $a_{ij}$ , are related to the elastic properties of the material and

$$\begin{aligned} \varepsilon_1 &= \varepsilon_{11}, \quad \varepsilon_2 = \varepsilon_{22}, \quad \varepsilon_3 = \varepsilon_{33}, \\ \varepsilon_4 &= 2\varepsilon_{23}, \quad \varepsilon_5 = 2\varepsilon_{13}, \quad \varepsilon_6 = 2\varepsilon_{12}, \\ \sigma_1 &= \sigma_{11}, \quad \sigma_2 = \sigma_{22}, \quad \sigma_3 = \sigma_{33}, \\ \sigma_4 &= \sigma_{23}, \quad \sigma_5 = \sigma_{13}, \quad \sigma_6 = \sigma_{12} \end{aligned} \quad (3)$$

For the special case of plane problems where at each point there is a plane of symmetry parallel to the surface of a thin plate in plane stress or plane strain, Eq. (2) can be reduced to six independent elastic constants for plane stress:

$$a_{ij} \quad (i, j = 1, 2, 6) \quad (4)$$

and six corresponding constants for plane strain:

$$b_{ij} = a_{ij} - \frac{a_{i3}a_{j3}}{a_{33}} \quad (i, j = 1, 2, 6) \quad (5)$$

Fig. 1 shows a crack tip referred to the Cartesian coordinate system in orthotropic FGMs. Two-dimensional anisotropic elasticity problems can be formulated in terms of the analytic functions,  $\phi_k(z_k)$ , of the complex variable,  $z_k = x_k + iy_k$  ( $k = 1, 2$ ), where

$$x_k = x + \alpha_k y, \quad y_k = \beta_k y \quad (k = 1, 2) \quad (6)$$

The parameters  $\alpha_k$  and  $\beta_k$  are the real and imaginary parts of  $\mu_k = \alpha_k + i\beta_k$ , which can be determined from the characteristic equation (Sih et al., 1965)

$$a_{11}\mu^4 - 2a_{16}\mu^3 + (2a_{12} + a_{66})\mu^2 - 2a_{26}\mu + a_{22} = 0 \quad (7)$$

The roots  $\mu_k$  are always complex or purely imaginary in conjugate pairs as  $\mu_1, \bar{\mu}_1; \mu_2, \bar{\mu}_2$ . Moreover,  $\mu_1$  and  $\mu_2$  must be evaluated at the crack-tip location for FGMs.

For mixed mode, the stresses in the vicinity of the crack tip are

---


$$\begin{aligned} \sigma_{11} &= \frac{K_I}{\sqrt{2\pi r}} \operatorname{Re} \left[ \frac{\mu_1^{\text{tip}} \mu_2^{\text{tip}}}{\mu_1^{\text{tip}} - \mu_2^{\text{tip}}} \left\{ \frac{\mu_2^{\text{tip}}}{\sqrt{\cos \theta + \mu_2^{\text{tip}} \sin \theta}} - \frac{\mu_1^{\text{tip}}}{\sqrt{\cos \theta + \mu_1^{\text{tip}} \sin \theta}} \right\} \right] \\ &+ \frac{K_{II}}{\sqrt{2\pi r}} \operatorname{Re} \left[ \frac{1}{\mu_1^{\text{tip}} - \mu_2^{\text{tip}}} \left\{ \frac{(\mu_2^{\text{tip}})^2}{\sqrt{\cos \theta + \mu_2^{\text{tip}} \sin \theta}} - \frac{(\mu_1^{\text{tip}})^2}{\sqrt{\cos \theta + \mu_1^{\text{tip}} \sin \theta}} \right\} \right] + \sigma_{11}^0 + \dots \\ \sigma_{22} &= \frac{K_I}{\sqrt{2\pi r}} \operatorname{Re} \left[ \frac{1}{\mu_1^{\text{tip}} - \mu_2^{\text{tip}}} \left\{ \frac{\mu_1^{\text{tip}}}{\sqrt{\cos \theta + \mu_2^{\text{tip}} \sin \theta}} - \frac{\mu_2^{\text{tip}}}{\sqrt{\cos \theta + \mu_1^{\text{tip}} \sin \theta}} \right\} \right] \\ &+ \frac{K_{II}}{\sqrt{2\pi r}} \operatorname{Re} \left[ \frac{1}{\mu_1^{\text{tip}} - \mu_2^{\text{tip}}} \left\{ \frac{1}{\sqrt{\cos \theta + \mu_2^{\text{tip}} \sin \theta}} - \frac{1}{\sqrt{\cos \theta + \mu_1^{\text{tip}} \sin \theta}} \right\} \right] + \sigma_{22}^0 \\ \sigma_{12} &= \frac{K_I}{\sqrt{2\pi r}} \operatorname{Re} \left[ \frac{\mu_1^{\text{tip}} \mu_2^{\text{tip}}}{\mu_1^{\text{tip}} - \mu_2^{\text{tip}}} \left\{ \frac{1}{\sqrt{\cos \theta + \mu_1^{\text{tip}} \sin \theta}} - \frac{1}{\sqrt{\cos \theta + \mu_2^{\text{tip}} \sin \theta}} \right\} \right] \\ &+ \frac{K_{II}}{\sqrt{2\pi r}} \operatorname{Re} \left[ \frac{1}{\mu_1^{\text{tip}} - \mu_2^{\text{tip}}} \left\{ \frac{\mu_1^{\text{tip}}}{\sqrt{\cos \theta + \mu_1^{\text{tip}} \sin \theta}} - \frac{\mu_2^{\text{tip}}}{\sqrt{\cos \theta + \mu_2^{\text{tip}} \sin \theta}} \right\} \right] + \sigma_{12}^0 \end{aligned} \quad (8)$$

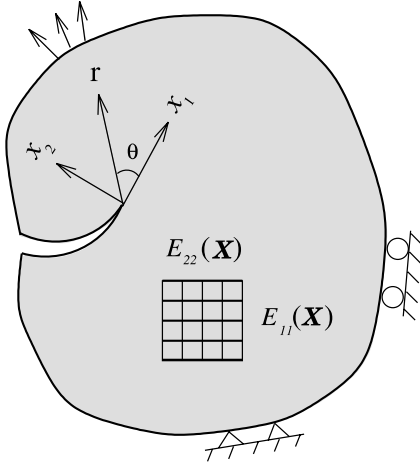


Fig. 1. Coordinate systems at the crack tip for orthotropic FGMs.

where  $\sigma_{11}^0$  is  $O(1)$  and the displacements are

$$\begin{aligned}
 u_1 &= K_I \sqrt{\frac{2r}{\pi}} \operatorname{Re} \left[ \frac{1}{\mu_1^{\text{tip}} - \mu_2^{\text{tip}}} \mu_1^{\text{tip}} p_2 \sqrt{\cos \theta + \mu_2^{\text{tip}} \sin \theta} - \mu_2^{\text{tip}} p_1 \sqrt{\cos \theta + \mu_1^{\text{tip}} \sin \theta} \right] \\
 &\quad + K_{II} \sqrt{\frac{2r}{\pi}} \operatorname{Re} \left[ \frac{1}{\mu_1^{\text{tip}} - \mu_2^{\text{tip}}} p_2 \sqrt{\cos \theta + \mu_2^{\text{tip}} \sin \theta} - p_1 \sqrt{\cos \theta + \mu_1^{\text{tip}} \sin \theta} \right] + \dots \\
 u_2 &= K_I \sqrt{\frac{2r}{\pi}} \operatorname{Re} \left[ \frac{1}{\mu_1^{\text{tip}} - \mu_2^{\text{tip}}} \mu_1^{\text{tip}} q_2 \sqrt{\cos \theta + \mu_2^{\text{tip}} \sin \theta} - \mu_2^{\text{tip}} q_1 \sqrt{\cos \theta + \mu_1^{\text{tip}} \sin \theta} \right] \\
 &\quad + K_{II} \sqrt{\frac{2r}{\pi}} \operatorname{Re} \left[ \frac{1}{\mu_1^{\text{tip}} - \mu_2^{\text{tip}}} q_2 \sqrt{\cos \theta + \mu_2^{\text{tip}} \sin \theta} - q_1 \sqrt{\cos \theta + \mu_1^{\text{tip}} \sin \theta} \right] + \dots
 \end{aligned} \tag{9}$$

where  $\mu_1^{\text{tip}}$  and  $\mu_2^{\text{tip}}$  denote the crack-tip material parameters calculated according to Eq. (7), i.e.  $\mu_1^{\text{tip}}$  and  $\mu_2^{\text{tip}}$  are the roots of Eq. (7), which are taken such that  $\beta_k > 0$  ( $k = 1, 2$ ), and  $p_k$  and  $q_k$  are given by

$$\begin{aligned}
 p_k &= a_{11} (\mu_k^{\text{tip}})^2 + a_{12} - a_{16} \mu_k^{\text{tip}} \\
 q_k &= a_{12} \mu_k^{\text{tip}} + \frac{a_{22}}{\mu_k^{\text{tip}}} - a_{26}
 \end{aligned} \tag{10}$$

respectively. Notice that the main difference between the above expressions for the crack-tip fields and those reported by Sih et al. (1965) is that here the material parameters are sampled at the crack-tip location.

### 3. $J_k^*$ -integral formulation for orthotropic FGMs

This section presents the derivation (for two-dimensional problems) of the  $J_k^*$ -integral for non-homogeneous orthotropic materials and details the actual FEM implementation. The spatial variation of material properties is considered, which includes elastic moduli  $E_{11} \equiv E_{11}(\mathbf{x})$ ,  $E_{22} \equiv E_{22}(\mathbf{x})$ ; in-plane shear modulus  $G_{12} \equiv G_{12}(\mathbf{x})$ ; and Poisson's ratio  $\nu_{12} \equiv \nu_{12}(\mathbf{x})$ . The EDI concept is used to evaluate  $J_k^*$  ( $k = 1, 2$ ) in the FEM implementation. The following derivation is an extension of the  $J_k^*$  formulation for isotropic FGMs (Eischen, 1987; Kim and Paulino, 2002a).

#### 3.1. Formulation

In an elastic FGM body subjected to two-dimensional deformation fields (plane strain, gen-

eralized plane stress), the strain energy density  $W$  is defined by

$$W = W(\varepsilon_{ij}, x_i) \quad \text{where } \sigma_{ij} = \frac{\partial W}{\partial \varepsilon_{ij}} \quad (i, j = 1, 2) \tag{11}$$

Thus the gradient of  $W$  is evaluated as

$$\begin{aligned}
 \nabla W &= \frac{\partial W}{\partial x_k} = \frac{\partial W}{\partial \varepsilon_{ij}} \frac{\partial \varepsilon_{ij}}{\partial x_k} + \left( \frac{\partial W}{\partial x_k} \right)_{\text{expl}} \\
 &= \sigma_{ij} \varepsilon_{ij,k} + (W_{,k})_{\text{expl}}
 \end{aligned} \tag{12}$$

where  $(\cdot)_{,k} \equiv \partial(\cdot)/\partial x_k$ , and the ‘‘explicit’’ derivative of  $W$  is defined by

$$\left(\frac{\partial W}{\partial x_k}\right)_{\text{expl}} = \frac{\partial}{\partial x_k} W(\varepsilon_{ij}, x_i)|_{\varepsilon_{ij}=\text{const.}, x_m=\text{const. for } m \neq k} \quad (13)$$

The symmetry properties of the stress tensor, the linearized strain–displacement relation, and the equilibrium equations lead to

$$(W\delta_{jk} - \sigma_{ij}u_{i,k})_{,j} - (W_{,k})_{\text{expl}} = 0 \quad (14)$$

where  $\delta_{jk}$  is the Kronecker delta. This expression represents a conservation law, valid pointwise, for an elastic FGM, free of body forces. Applying the divergence theorem to Eq. (14), one obtains

$$\oint_{\Gamma} (Wn_k - \sigma_{ij}n_j u_{i,k}) d\Gamma - \int_{\Omega} (W_{,k})_{\text{expl}} d\Omega = 0 \quad (15)$$

where  $\Gamma$  is a simple closed curve in the  $(x_1, x_2)$  local coordinates,  $\Omega$  is the domain enclosed by  $\Gamma$ , and  $n_j$  is the outward unit normal vector to  $\Gamma$ .

Because the stress and strain fields are singular and unbounded at the crack tip, a special region  $\Omega$  in Eq. (15) must be considered such that the region does not contain the crack tip. Fig. 2 shows a crack located in a two-dimensional body of arbitrary shape. The region  $\Omega$  (free of singularity) is bounded by a closed curve  $\Gamma$  including segments  $\Gamma_0, \Gamma_c^+, \Gamma_\varepsilon,$  and  $\Gamma_c^-$ . The region between  $\Gamma_\varepsilon$  and the crack surfaces is  $\Omega_\varepsilon$ . The region  $\Omega_0$  is defined as

$\Omega + \Omega_\varepsilon$ . The divergence theorem can be applied in the region  $\Omega$ . By using the expression

$$\Gamma = \Gamma_0 + \Gamma_c^+ + \Gamma_\varepsilon + \Gamma_c^- \quad (16)$$

Eq. (15) leads to

$$\int_{\Gamma_0} b_k d\Gamma + \int_{\Gamma_c^+} b_k d\Gamma + \int_{\Gamma_\varepsilon} b_k d\Gamma + \int_{\Gamma_c^-} b_k d\Gamma - \int_{\Omega} (W_{,k})_{\text{expl}} d\Omega = 0 \quad (17)$$

where

$$b_k = Wn_k - \sigma_{ij}n_j u_{i,k} \quad (18)$$

Reversing the integration path in the third term of Eq. (17), and decomposing the region  $\Omega$  into  $\Omega_0 - \Omega_\varepsilon$ , i.e.  $\Omega = \Omega_0 - \Omega_\varepsilon$ , one obtains

$$\int_{\Gamma_0} b_k d\Gamma - \int_{\Omega_0} (W_{,k})_{\text{expl}} d\Omega + \int_{\Gamma_c^+} b_k d\Gamma + \int_{\Gamma_c^-} b_k d\Gamma = \int_{\Gamma_\varepsilon} b_k d\Gamma - \int_{\Omega_\varepsilon} (W_{,k})_{\text{expl}} d\Omega \quad (19)$$

By taking the limit  $\Gamma_\varepsilon \rightarrow 0$  of the right-hand-side of Eq. (19), a vector  $J_k^*$  is introduced as

$$J_k^* \equiv \lim_{\Gamma_\varepsilon \rightarrow 0} \left[ \int_{\Gamma_\varepsilon} b_k d\Gamma - \int_{\Omega_\varepsilon} (W_{,k})_{\text{expl}} d\Omega \right] \quad (20)$$

As the loop  $\Gamma_\varepsilon$  is closer to the crack tip, the domain integral in Eq. (20) vanishes because derivatives of the elastic moduli are bounded at the crack tip. Then Eqs. (19) and (20) lead to

$$J_k^* \equiv \lim_{\Gamma_\varepsilon \rightarrow 0} \int_{\Gamma_\varepsilon} b_k d\Gamma \quad (21)$$

and thus

$$J_k^* \equiv \lim_{\Gamma_\varepsilon \rightarrow 0} \left\{ \int_{\Gamma_0} b_k d\Gamma - \int_{\Omega_0} (W_{,k})_{\text{expl}} d\Omega + \int_{\Gamma_c^+} b_k d\Gamma + \int_{\Gamma_c^-} b_k d\Gamma \right\} \quad (22)$$

Let us combine the two terms which involve integrations along two crack faces, and define the associated path of integration as  $\Gamma_c$ , i.e.  $\Gamma_c = \Gamma_c^+ + \Gamma_c^-$ . For the sake of the derivation given later, the path  $\Gamma_0$  intersects the top and bottom crack faces at the same distance from the crack tip, as shown in Fig. 2. Eq. (22) together with Eq. (18) lead to the general expression

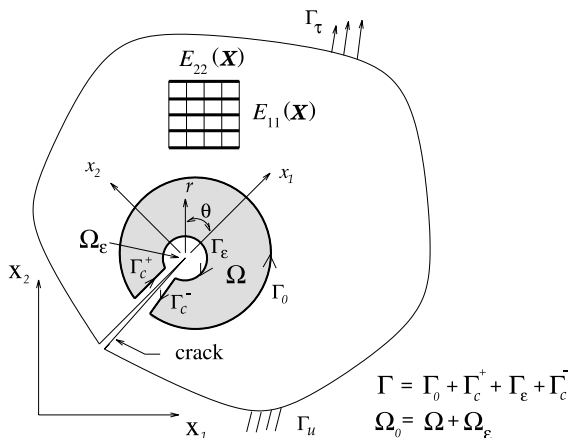


Fig. 2. Schematic of a cracked body and notation.

$$J_k^* = \lim_{\Gamma_\varepsilon \rightarrow 0} \left\{ \int_{\Gamma_0} [W n_k - \sigma_{ij} n_j u_{i,k}] d\Gamma - \int_{\Omega_0} (W_{,k})_{\text{expl}} d\Omega + \int_{\Gamma_c} ([W^+ - W^-] n_k^+ - [t_i^+ u_{i,k}^+ - t_i^- u_{i,k}^-]) d\Gamma \right\} \quad (23)$$

where  $t_i = \sigma_{ij} n_j$ , (+) and (−) refer to the upper and lower crack faces, and  $n_k^+ = -n_k^-$  is the outward unit normal vector to  $\Gamma_c^+$ . The notation  $[W^+ - W^-]$  denotes the discontinuity (or jump) in the strain energy density across the crack faces. Notice that the material nonhomogeneity affects the standard  $J$ -integral (Rice, 1968) by adding a domain integral term. *This term must be taken into account in order to evaluate the  $J$ -integral in FGMs.*

The closed contour integral of Eq. (23) is converted into an EDI (Gu et al., 1999; Raju, 1990) for traction-free crack faces:

$$J_k^* = \int_A [\sigma_{ij} u_{i,k} - W \delta_{kj}] q_{,j} dA - \int_A (W_{,k})_{\text{expl}} q dA + \int_{\Gamma_c} [W^+ - W^-] q n_k^+ d\Gamma \quad (24)$$

where  $q$  is a smooth function which changes from unity on  $\Gamma_\varepsilon$  to zero on  $\Gamma_0$ . The plateau function was adopted in the present finite element analysis, as illustrated by Fig. 3. The last term of Eq. (24) is defined as

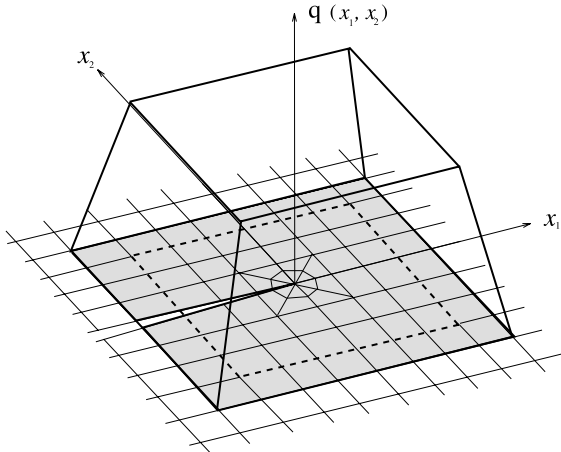


Fig. 3. Plateau  $q$  function (weight function).

$$R = \int_{\Gamma_c} [W^+ - W^-] q n_k^+ d\Gamma \quad (25)$$

where the strain energy density can be represented for generalized plane stress as

$$W = W[E_{11}(\mathbf{x}), E_{22}(\mathbf{x}), G_{12}(\mathbf{x}), v_{12}(\mathbf{x}), \varepsilon(\mathbf{x})] \quad (26)$$

with  $\mathbf{x} = (x_1, x_2)$ . Thus the explicit derivative of  $W$  in the second term of Eq. (24) becomes

$$\left( \frac{\partial W}{\partial x_k} \right)_{\text{expl}} = \frac{\partial W}{\partial E_{11}} \frac{\partial E_{11}}{\partial x_k} + \frac{\partial W}{\partial E_{22}} \frac{\partial E_{22}}{\partial x_k} + \frac{\partial W}{\partial G_{12}} \frac{\partial G_{12}}{\partial x_k} + \frac{\partial W}{\partial v_{12}} \frac{\partial v_{12}}{\partial x_k} \quad (27)$$

It is worth mentioning that if the material properties are given by a known function, e.g. exponential (Ozturk and Erdogan, 1997, 1999), then the expression (27) can be evaluated in closed form. However, if such is not the case, e.g. when the properties are obtained from micromechanics models (Reiter et al., 1997; Zuiker, 1995), then the expression (27) needs to be evaluated numerically.

If we separate Eq. (24) into mode I and mode II contributions, then for mode I ( $k = 1$  in Eq. (24)),

$$(J_1^*)_{\text{local}} = \int_A [\sigma_{ij} u_{i,1} - W \delta_{1j}] q_{,j} dA - \int_A (W_{,1}) q dA \quad (28)$$

and for mode II ( $k = 2$  in Eq. (24)),

$$(J_2^*)_{\text{local}} = \int_A [\sigma_{ij} u_{i,2} - W \delta_{2j}] q_{,j} dA - \int_A (W_{,2}) q dA + \int_{\Gamma_c} [W^+ - W^-] q n_2^+ d\Gamma \quad (29)$$

Notice that the expression for  $(J_2^*)_{\text{local}}$  given in Eq. (29) includes the  $R$  term of Eq. (25), which is the integration along the crack faces of the discontinuity in the strain energy density; while the expression for  $(J_1^*)_{\text{local}}$  does not. The  $R$  term causes difficulty in the numerical evaluation of  $(J_2^*)_{\text{local}}$  (Kim and Paulino, 2002a). In what follows, it is useful to derive an expression for  $[W^+ - W^-]$  near a crack tip.

Recall that for orthotropic FGMs in plane stress ( $E_{11} \equiv E_{11}(\mathbf{x})$ ,  $E_{22} \equiv E_{22}(\mathbf{x})$ ,  $G_{12} \equiv G_{12}(\mathbf{x})$ ,  $\nu_{12} \equiv \nu_{12}(\mathbf{x})$ ), the strain energy density is given by

$$W = \frac{1}{2} \left( \frac{\sigma_{11}^2}{E_{11}(\mathbf{x})} + \frac{\sigma_{22}^2}{E_{22}(\mathbf{x})} - \frac{2\nu_{12}(\mathbf{x})}{E_{11}(\mathbf{x})} \sigma_{11}\sigma_{22} + \frac{1}{G_{12}(\mathbf{x})} \sigma_{12}^2 \right) \quad (30)$$

Evaluation of Eq. (8) for  $\theta = \pm\pi$  yields

$$\begin{aligned} \sigma_{11}(r, +\pi) &= \frac{K_I}{\sqrt{2\pi r}} \{-A(\beta_1 - \beta_2) - B(\alpha_1 - \alpha_2)\} \\ &\quad + \frac{K_{II}}{\sqrt{2\pi r}} \{2C(\alpha_2\beta_2 - \alpha_1\beta_1) \\ &\quad - D(\alpha_1^2 - \alpha_2^2 - \beta_1^2 + \beta_2^2)\} + \sigma_{11}^0 \\ \sigma_{22}(r, +\pi) &= \frac{K_I}{\sqrt{2\pi r}} \{C(\beta_1 - \beta_2) + D(\alpha_1 - \alpha_2)\} \\ \sigma_{12}(r, +\pi) &= \frac{K_{II}}{\sqrt{2\pi r}} \{C(\beta_1 - \beta_2) + D(\alpha_1 - \alpha_2)\} \\ \sigma_{11}(r, -\pi) &= -\sigma_{11}(r, \pi) + 2\sigma_{11}^0 \\ \sigma_{22}(r, -\pi) &= -\sigma_{22}(r, \pi) \\ \sigma_{12}(r, -\pi) &= -\sigma_{12}(r, \pi) \end{aligned} \quad (31)$$

where

$$A = \frac{(\alpha_1 - \alpha_2)(\alpha_1\alpha_2 - \beta_1\beta_2) + (\beta_1 - \beta_2)(\alpha_2\beta_1 + \alpha_1\beta_2)}{(\alpha_1 - \alpha_2)^2 + (\beta_1 - \beta_2)^2}$$

$$B = \frac{(\alpha_1 - \alpha_2)(\alpha_2\beta_1 + \alpha_1\beta_2) - (\beta_1 - \beta_2)(\alpha_1\alpha_2 - \beta_1\beta_2)}{(\alpha_1 - \alpha_2)^2 + (\beta_1 - \beta_2)^2}$$

$$C = \frac{\alpha_1 - \alpha_2}{(\alpha_1 - \alpha_2)^2 + (\beta_1 - \beta_2)^2}$$

$$D = \frac{\beta_2 - \beta_1}{(\alpha_1 - \alpha_2)^2 + (\beta_1 - \beta_2)^2}$$

Thus, performing some algebraic manipulation in Eq. (30), one obtains

$$\begin{aligned} W(r, \pi) - W(r, -\pi) &= [W^+ - W^-] \\ &= \frac{K_I}{\sqrt{2\pi r}} \left[ \left\{ \frac{2\sigma_{11}^0}{E_{11}(r)} \right\} \{-A(\beta_1 - \beta_2) - B(\alpha_1 - \alpha_2)\} + \left\{ -\frac{2\nu_{12}(r)\sigma_{11}^0}{E_{11}(r)} \right\} \right. \\ &\quad \times \{C(\beta_1 - \beta_2) + D(\alpha_1 - \alpha_2)\} \left. \right] \\ &\quad + \frac{K_{II}}{\sqrt{2\pi r}} \left[ \left\{ \frac{2\sigma_{11}^0}{E_{11}(r)} \right\} \right. \\ &\quad \times \{2C(\alpha_2\beta_2 - \alpha_1\beta_1) - D(\alpha_1^2 - \alpha_2^2 - \beta_1^2 + \beta_2^2)\} \left. \right] \\ &\quad + O(r^{1/2}) + \dots \end{aligned} \quad (32)$$

which can be rewritten as

$$[W^+ - W^-] = \frac{1}{\sqrt{2\pi r}} F(K_I, K_{II}, \sigma_{11}^0, \sigma_{22}^0, \sigma_{12}^0, E_{11}(r), E_{22}(r), G_{12}(r), \nu_{12}(r)) + O(r^{1/2}) \quad (33)$$

where  $F = F(K_I, K_{II}, \sigma_{11}^0, E_{11}(r), E_{22}(r), G_{12}(r), \nu_{12}(r))$ . The range of integration can be divided into two parts: the first remote from the crack tip, and the second close to the crack tip. Thus a characteristic distance parameter is introduced, which is denoted  $\delta$ , as shown in Fig. 4. The origin of the  $x_1$  axis will be located at the point where the path  $\Gamma_0$  intersects the crack face. The distance from this point to the crack tip is  $d$ . It will be assumed that over the distance  $\delta$ , the term

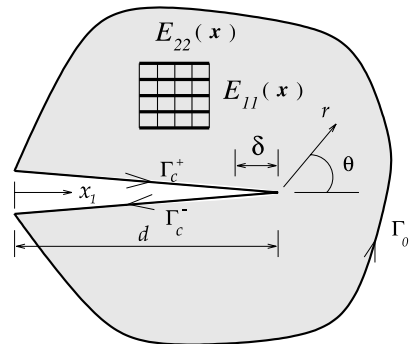


Fig. 4. Schematic of the integration path and establishment of notation.

$[W^+ - W^-]$  is satisfactorily approximated by the asymptotic form above (see Eq. (32)). The following approximation is made to the integration of  $[W^+ - W^-]$  along the crack face

$$\begin{aligned} \int_{\Gamma_c} [W^+ - W^-] q n_2^+ d\Gamma &= - \int_{\Gamma_c} [W^+ - W^-] q dx_1 \\ &\approx - \int_0^{d-\delta} [W^+ - W^-] q dx_1 - \int_{d-\delta}^d \frac{F}{\sqrt{2\pi r}} q dx_1 \end{aligned} \quad (34)$$

Using the fact that along the crack face  $r = d - x_1$  (see Fig. 4), one rewrites Eq. (34) as

$$\begin{aligned} \int_{\Gamma_c} [W^+ - W^-] q n_2^+ d\Gamma \\ \approx - \int_0^{d-\delta} [W^+ - W^-] q dx_1 - \frac{2\sqrt{\delta}}{\sqrt{2\pi}} F \end{aligned} \quad (35)$$

where  $F \equiv F^{\text{tip}} = F(K_I, K_{II}, \sigma_{11}^0, E_{11}^{\text{tip}}, E_{22}^{\text{tip}}, G_{12}^{\text{tip}}, \nu_{12}^{\text{tip}})$ . Thus, based on Eq. (29) and using the result given by Eq. (35), the approximate expression for  $(J_2^*)_{\text{local}}$  is

$$\begin{aligned} (J_2^*)_{\text{local}} &\approx \int_A [\sigma_{ij} u_{i,2} - W \delta_{2j}] q_{,j} dA \\ &\quad - \int_A (W_{,2}) q dA - \int_0^{d-\delta} [W^+ - W^-] q dx_1 \\ &\quad - \frac{2\sqrt{\delta}}{\sqrt{2\pi}} F \end{aligned} \quad (36)$$

If the crack faces are traction free, an expression for the strain energy density can be obtained according to the global coordinates  $(X_1, X_2)$

$$W = \frac{1}{2}(\sigma_{11}\varepsilon_{11} + \sigma_{22}\varepsilon_{22} + \sigma_{12}\varepsilon_{12}) \quad (37)$$

as used in the FEM implementation. The strain and stress values are evaluated directly on the crack faces ( $\Gamma_c^+$  and  $\Gamma_c^-$ ) using Gauss integration along the 3-node line segments of the parent elements (T6, Q8), rather than being smoothed from the element interiors. This procedure improves the accuracy of the numerical results (Kim and Paulino, 2002a).

### 3.2. Numerical aspects

Since the FEM calculations of displacement, strain, stress, etc., are based on the global co-

ordinate system, the  $(J_k^*)_{\text{global}}$  is evaluated first and then transformed into  $(J_k^*)_{\text{local}}$ . The quantity  $(\hat{J}_2^*)_{\text{local}}$  is introduced from Eq. (36) as

$$\begin{aligned} (\hat{J}_2^*)_{\text{local}} &\approx \int_A [\sigma_{ij} u_{i,2} - W \delta_{2j}] q_{,j} dA - \int_A (W_{,2}) q dA \\ &\quad - \int_0^{d-\delta} [W^+ - W^-] q dx_1 \end{aligned} \quad (38)$$

so that

$$(J_2^*)_{\text{local}} = (\hat{J}_2^*)_{\text{local}} - \frac{2\sqrt{\delta}}{\sqrt{2\pi}} F \quad (39)$$

or

$$(\hat{J}_2^*)_{\text{local}} = (J_2^*)_{\text{local}} + \frac{2\sqrt{\delta}}{\sqrt{2\pi}} F \quad (40)$$

The above expressions are represented by the local coordinates  $x_k$ , which can be expressed in terms of the global coordinates  $X_i$  by the usual transformation

$$x_i = \alpha_{ij}(\theta) X_j, \quad \alpha_{ij}(\theta) = \begin{bmatrix} \cos \theta & \sin \theta \\ -\sin \theta & \cos \theta \end{bmatrix} \quad (41)$$

The same transformation also holds for the  $J_k^*$  integral, i.e.

$$\begin{Bmatrix} (J_1^*)_{\text{local}} \\ (J_2^*)_{\text{local}} \end{Bmatrix} = \begin{bmatrix} \cos \theta & \sin \theta \\ -\sin \theta & \cos \theta \end{bmatrix} \begin{Bmatrix} (J_1^*)_{\text{global}} \\ (J_2^*)_{\text{global}} \end{Bmatrix} \quad (42)$$

For the sake of numerical implementation by the FEM, Eq. (24) is evaluated in global coordinates. Thus

$$(J_1^*)_{\text{global}} = (\tilde{J}_1^*)_{\text{global}} - R \sin \theta \quad (43)$$

$$(J_2^*)_{\text{global}} = (\tilde{J}_2^*)_{\text{global}} + R \cos \theta \quad (44)$$

where

$$\begin{aligned} (\tilde{J}_1^*)_{\text{global}} &= \int_A \left[ \sigma_{ij} \frac{\partial u}{\partial X_1} - W \delta_{1j} \right] \frac{\partial q}{\partial X_j} dA \\ &\quad - \int_A \left( \frac{\partial W}{\partial X_1} \right) q dA \end{aligned} \quad (45)$$

$$\begin{aligned} (\tilde{J}_2^*)_{\text{global}} &= \int_A \left[ \sigma_{ij} \frac{\partial u}{\partial X_2} - W \delta_{2j} \right] \frac{\partial q}{\partial X_j} dA \\ &\quad - \int_A \left( \frac{\partial W}{\partial X_2} \right) q dA \end{aligned} \quad (46)$$

The defined quantities  $(\tilde{J}_1^*)_{\text{global}}$  (Eq. (45)) and  $(\tilde{J}_2^*)_{\text{global}}$  (Eq. (46)) are computed numerically to calculate  $(J_1^*)_{\text{local}}$  according to the transformation given by Eq. (42), i.e.

$$(J_1^*)_{\text{local}} = (\tilde{J}_1^*)_{\text{global}} \cos \theta + (\tilde{J}_2^*)_{\text{global}} \sin \theta \quad (47)$$

The quantity  $(\hat{J}_2^*)_{\text{local}}$  is computed using Eq. (38), for two values of  $\delta$  ( $\delta_1, \delta_2$ ). These values of  $(\hat{J}_2^*)_{\text{local}}$  are called  $(\hat{J}_2^*)_{\delta_1}$ , and  $(\hat{J}_2^*)_{\delta_2}$ . Therefore, from Eq. (40), one obtains

$$(\hat{J}_2^*)_{\delta_1} = (J_2^*)_{\text{local}} + \frac{2\sqrt{\delta_1}}{\sqrt{2\pi}} F \quad (48)$$

$$(\hat{J}_2^*)_{\delta_2} = (J_2^*)_{\text{local}} + \frac{2\sqrt{\delta_2}}{\sqrt{2\pi}} F \quad (49)$$

Once  $(J_1^*)_{\text{local}}$ ,  $(\hat{J}_2^*)_{\delta_1}$ , and  $(\hat{J}_2^*)_{\delta_2}$  have been computed numerically, the  $(J_2^*)_{\text{local}}$  is obtained as follows:

$$(J_2^*)_{\text{local}} = \frac{(\hat{J}_2^*)_{\delta_1} \sqrt{\delta_2} - (\hat{J}_2^*)_{\delta_2} \sqrt{\delta_1}}{\sqrt{\delta_2} - \sqrt{\delta_1}} \quad (50)$$

The relationship between the two components of the  $J_k^*$ -integral and the mode I and mode II SIFs is established as (Obata et al., 1989; Ma and Chen, 1996)

$$(J_1^*)_{\text{local}} = -\frac{a_{11}}{2} \text{Im} \left[ K_I^2 (\mu_1^{\text{tip}} + \mu_2^{\text{tip}}) \overline{\mu_1^{\text{tip}} \mu_2^{\text{tip}}} + 2K_I K_{II} \overline{\mu_1^{\text{tip}} \mu_2^{\text{tip}}} - K_{II}^2 (\mu_1^{\text{tip}} + \mu_2^{\text{tip}}) \right] \quad (51)$$

$$(J_2^*)_{\text{local}} = -\frac{a_{11}}{4} \text{Im} \left[ K_I^2 (\mu_1^{\text{tip}} \mu_2^{\text{tip}} + \overline{\mu_1^{\text{tip}} \mu_2^{\text{tip}}}) \overline{\mu_1^{\text{tip}} \mu_2^{\text{tip}}} - K_I K_{II} \left\{ \mu_1^{\text{tip}} \mu_2^{\text{tip}} (\mu_1^{\text{tip}} + \mu_2^{\text{tip}} + \overline{\mu_1^{\text{tip}}} + \overline{\mu_2^{\text{tip}}}) + (\mu_1^{\text{tip}} + \mu_2^{\text{tip}}) (\mu_1^{\text{tip}} \mu_2^{\text{tip}} + 3\overline{\mu_1^{\text{tip}} \mu_2^{\text{tip}}}) \right\} + K_{II}^2 \left\{ \mu_1^{\text{tip}} \mu_2^{\text{tip}} (\mu_1^{\text{tip}} + \mu_2^{\text{tip}} + \overline{\mu_1^{\text{tip}}} + \overline{\mu_2^{\text{tip}}}) + \overline{\mu_1^{\text{tip}} \mu_2^{\text{tip}}} \right\} \right] \quad (52)$$

For this case, the SIFs are coupled and they may be solved by means of the Newton iteration algorithm with the system of nonlinear equations as follows:

$$\mathbf{F}(\mathbf{K}) = (F_1(\mathbf{K}), F_2(\mathbf{K})),$$

$$F_1(\mathbf{K}) = (J_1^*)_{\text{local}} + \frac{a_{11}}{2} \times \text{Im} \left[ K_I^2 (\mu_1^{\text{tip}} + \mu_2^{\text{tip}}) \overline{\mu_1^{\text{tip}} \mu_2^{\text{tip}}} + 2K_I K_{II} \overline{\mu_1^{\text{tip}} \mu_2^{\text{tip}}} - K_{II}^2 (\mu_1^{\text{tip}} + \mu_2^{\text{tip}}) \right]$$

$$F_2(\mathbf{K}) = (J_2^*)_{\text{local}} + \frac{a_{11}}{4} \times \text{Im} \left[ K_I^2 (\mu_1^{\text{tip}} \mu_2^{\text{tip}} + \overline{\mu_1^{\text{tip}} \mu_2^{\text{tip}}}) \overline{\mu_1^{\text{tip}} \mu_2^{\text{tip}}} - K_I K_{II} \left\{ \mu_1^{\text{tip}} \mu_2^{\text{tip}} (\mu_1^{\text{tip}} + \mu_2^{\text{tip}} + \overline{\mu_1^{\text{tip}}} + \overline{\mu_2^{\text{tip}}}) + (\mu_1^{\text{tip}} + \mu_2^{\text{tip}}) (\mu_1^{\text{tip}} \mu_2^{\text{tip}} + 3\overline{\mu_1^{\text{tip}} \mu_2^{\text{tip}}}) \right\} + K_{II}^2 \left\{ \mu_1^{\text{tip}} \mu_2^{\text{tip}} (\mu_1^{\text{tip}} + \mu_2^{\text{tip}} + \overline{\mu_1^{\text{tip}}} + \overline{\mu_2^{\text{tip}}}) + \overline{\mu_1^{\text{tip}} \mu_2^{\text{tip}}} \right\} \right] \quad (53)$$

where  $\mathbf{F}$  is a vector-valued function of  $F_1$  and  $F_2$ , and  $\mathbf{K}$  is a vector of the unknowns ( $K_I, K_{II}$ ).

*Determination of ( $K_I, K_{II}$ ) using Newton iteration:*

1. Select  $\mathbf{K}^{(0)}$  ( $K_I, K_{II}$ ) and initialize counter  $i = 0$ .
2. Compute gradient:  $\nabla \mathbf{F}(\mathbf{K})$ .
3. Perform iteration:  $\mathbf{K}^{(i+1)} = \mathbf{K}^{(i)} - \frac{\mathbf{F}(\mathbf{K}^{(i)})}{\nabla \mathbf{F}(\mathbf{K}^{(i)})}$ .
4. Check convergence: If  $|\mathbf{F}(\mathbf{K}^{(i)})| > \text{TOL}$ , then  $i \leftarrow i + 1$ , and GOTO Step 1.

For the initial values of  $\mathbf{K}^{(0)}$  ( $K_I, K_{II}$ ) in Step 1, we may use the SIFs obtained by the displacement correlation technique (DCT) because it provides physically reasonable SIF values and accelerates the iterative procedure. Any other judicious choice for the initial values of  $\mathbf{K}^{(0)}$  ( $K_I, K_{II}$ ) may be also acceptable. The SIFs obtained by the DCT are

$$K_I = \frac{1}{4} \sqrt{\frac{2\pi}{\Delta a} \frac{D(4u_{1,i-1} - u_{1,i-2}) - B(4u_{2,i-1} - u_{2,i-2})}{AD - BC}} \quad (54)$$

$$K_{II} = \frac{1}{4} \sqrt{\frac{2\pi}{\Delta a} \frac{A(4u_{2,i-1} - u_{2,i-2}) - C(4u_{1,i-1} - u_{1,i-2})}{AD - BC}} \quad (55)$$

where

$$A = \text{Re} \left[ \frac{i}{\mu_1^{\text{tip}} - \mu_2^{\text{tip}}} (\mu_1 p_2 - \mu_2 p_1) \right] \quad (56)$$

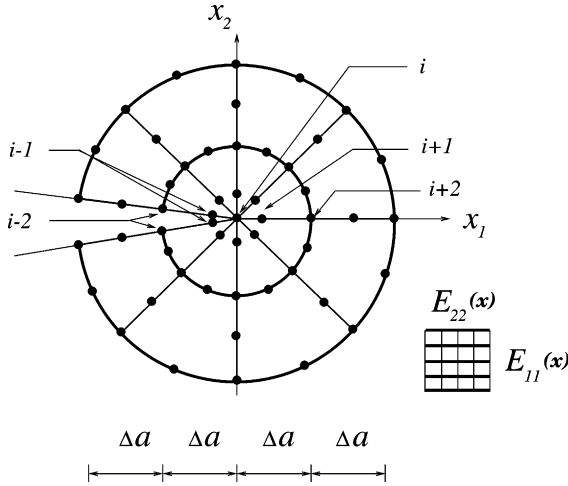


Fig. 5. Crack tip rosette of singular quarter-point (1st ring) and regular (2nd ring) finite elements. Notice that  $\mathbf{x} = (x_1, x_2)$ .

$$B = \text{Re} \left[ \frac{i}{\mu_1^{\text{tip}} - \mu_2^{\text{tip}}} (p_2 - p_1) \right] \quad (57)$$

$$C = \text{Re} \left[ \frac{i}{\mu_1^{\text{tip}} - \mu_2^{\text{tip}}} (\mu_1 q_2 - \mu_2 q_1) \right] \quad (58)$$

$$D = \text{Re} \left[ \frac{i}{\mu_1^{\text{tip}} - \mu_2^{\text{tip}}} (q_2 - q_1) \right] \quad (59)$$

in which  $u_{1,i-1}$ ,  $u_{1,i-2}$ ,  $u_{2,i-1}$ , and  $u_{2,i-2}$  are the relative displacements of the crack tip in the  $x_i$  ( $i = 1, 2$ ) direction at locations  $(i-1)$  and  $(i-2)$ ,  $r$  is the distance from the crack tip along the  $x_1$  direction,  $\Delta a$  is the characteristic length of the crack tip elements (see Fig. 5), and all the material parameters and related coefficients are considered at the crack tip location. The feasibility of the procedure explained above is illustrated by the numerical examples in Section 5.

#### 4. Finite element implementation

Graded elements are introduced to discretize functionally graded material properties (Kim and Paulino, 2002a,b). The material properties at

Gauss quadrature points are interpolated from the nodal material properties. The graded element were implemented according to the GIF described by Kim and Paulino (2002a,b). The behavior of graded elements (4-node and 8-node quadrilateral elements) has been studied by Paulino and Kim (submitted for publication) considering plane and axisymmetric states in isotropic FGMs. For the fracture analyses, the public domain FEM code FRANC2D (FRacture ANalysis Code 2D) (Wawrzynek, 1987; Wawrzynek and Ingraffea, 1991) has been used as the basis for implementing fracture capabilities in FGMs. The source code of FRANC2D is fully accessible which makes it ideal for further research and development. The extended code for FGMs is called I-FRANC2D (Illinois—FRANC2D). The I-FRANC2D has special techniques to evaluate SIFs in both isotropic and orthotropic FGMs (such as the  $J_k^*$ -integral), and to create many sectors and rings around a crack tip. At the crack tip, six-node triangular quarter-point (T6qp) singular elements are used; far away from the crack(s), eight-node serendipity elements (Q8) are used; and regular triangular quadratic elements (T6) are employed in the transition region between T6qp and Q8 elements. Thus the code allows a careful design of the mesh around the crack-tip region, which is especially beneficial for modeling orthotropic FGMs.

#### 5. Numerical examples

This paper examines, by means of computational experiments, the elastic stress analysis for orthotropic FGMs and the performance of the  $J_k^*$ -integral in computing SIFs using the FEM. In order to verify the performance of the  $J_k^*$ -integral, the following examples are considered:

1. Path-independence of  $J_k^*$ .
2. Plate with a crack parallel to the material gradation.
3. Plate with a crack perpendicular to the material gradation.
4. Poisson's ratio effect.

These problems assess the FEM code and the performance of the  $J_k^*$ -integral presented for evaluation of SIFs in orthotropic FGMs. For all the examples, the material property nonhomogeneity is expressed by a known function (see Eq. (27) and related comments). Moreover, all the examples have either numerical (e.g. finite element) or semi-analytical (e.g. integral equation method) solutions available. Thus, the results obtained with our I-FRANC2D code are compared with those available solutions.

The independent engineering constants  $E_{ii}$ ,  $G_{ij}$  and  $\nu_{ij}$  ( $(\nu_{ij}/E_{ii}) = (\nu_{ji}/E_{jj})$ ) ( $i, j = 1, 2, 3$ ) can be replaced by the averaged Young's modulus  $E$ , the effective Poisson's ratio  $\nu$ , the stiffness ratio  $\delta^4$  and the shear parameter  $\kappa_0$  (Krenk, 1979), i.e.

$$E = \sqrt{E_{11}E_{22}}, \quad \nu = \sqrt{\nu_{12}\nu_{21}}, \quad \delta^4 = \frac{E_{11}}{E_{22}} = \frac{\nu_{12}}{\nu_{21}},$$

$$\kappa_0 = \frac{E}{2G_{12}} - \nu \quad (60)$$

for generalized plane stress. Expressions for plane strain can be found in the paper by Krenk (1979). For the sake of comparison with semi-analytical solutions by Ozturk and Erdogan (1997, 1999), the above averaged parameters will be used in the second and third examples below. For plane orthotropy, the bounds on Poisson's ratios  $\nu_{12}$  and  $\nu_{21}$  are given by (Christensen, 1979):

$$|\nu_{12}| < (E_{11}/E_{22})^{1/2}, \quad |\nu_{21}| < (E_{22}/E_{11})^{1/2} \quad (61)$$

respectively. Therefore the bound on the effective Poisson's ratio is  $\nu < 1.0$ .

### 5.1. Path-independence of $J_k^*$

This example discusses path-independence of the  $J_k^*$ -integral (includes the explicit derivative of  $W$ ) in comparison with the  $J_k$ -integral (excludes the explicit derivative of  $W$ ). Fig. 6(a) shows a crack of length  $2a$  located with the angle  $\theta = 36^\circ$  in a finite two-dimensional plate under fixed-grip loading, Fig. 6(b) shows the complete finite element mesh, and Fig. 6(c) shows the contours used to evaluate both  $J_k^*$  and  $J_k$  ( $k = 1, 2$ ). Notice that the Young's modulus  $E(\mathbf{X})$  for the isotropic FGM case, and the material parameters  $E_{11}(\mathbf{X})$ ,  $E_{22}(\mathbf{X})$ , and  $G_{12}(\mathbf{X})$  for the orthotropic FGM case are

exponentially graded as functions of  $X_1$ , while the Poisson's ratio is constant for both cases. The displacement boundary conditions are prescribed such that  $u_1 = 0$  for the left corner node on the bottom edge, and  $u_2 = 0$  for all the nodes on the bottom edge. The applied load along the top edge corresponds to  $\sigma_{22}(X_1, X_2) = \sigma_{22}(-10 \leq X_1 \leq 10, 10) = \varepsilon_0 E^0 e^{\beta X_1}$  for the isotropic case and  $\sigma_{22}(-10 \leq X_1 \leq 10, 10) = \varepsilon_0 E_{22}^0 e^{\beta X_1}$  for the orthotropic case, as illustrated by Fig. 6(a), which shows a fixed-grip loading case.

The mesh has been discretized with 625 Q8, 176 T6, and 24 T6qp singular elements with a total of 825 elements and 2392 nodes (see Fig. 6(b)). Fig. 6(c) shows a detail around the crack-tip region with 4 rings (R4) and 12 sectors (S12) of elements. The following data were used for the FEM analysis:

$$a/W = 0.1, \quad L/W = 1.0, \quad \varepsilon_0 = 1.0$$

generalized plane stress,  $2 \times 2$  Gauss quadrature

For isotropic FGM case:

$$E(X_1) = E^0 e^{\beta X_1}, \quad E^0 = 1.0, \quad \nu = 0.3, \quad \beta a = 0.25$$

For orthotropic FGM case:

$$E_{11}(X_1) = E_{11}^0 e^{\alpha X_1}, \quad E_{22}(X_1) = E_{22}^0 e^{\beta X_1},$$

$$G_{12}(X_1) = G_{12}^0 e^{\gamma X_1}, \quad E_{11}^0 = 0.75,$$

$$E_{22}^0 = 1.0, \quad G_{12}^0 = 0.5,$$

$$\nu_{12} = 0.3, \quad (\alpha a, \beta a, \gamma a) = (0.2, 0.25, 0.15), \quad (62)$$

Notice that the independent nonhomogeneity parameters  $(\alpha, \beta, \gamma)$  are given by

$$\alpha = \frac{1}{2W} \log \left[ \frac{E_{11}(W)}{E_{11}(-W)} \right],$$

$$\beta = \frac{1}{2W} \log \left[ \frac{E_{22}(W)}{E_{22}(-W)} \right],$$

$$\gamma = \frac{1}{2W} \log \left[ \frac{G_{12}(W)}{G_{12}(-W)} \right] \quad (63)$$

and have units  $[\text{length}]^{-1}$ .

Figs. 7 and 8 show the path-independence of  $J_k^*$  ( $J_1^*, J_2^*$ ) in comparison with  $J_k$  ( $J_1, J_2$ ) in the isotropic and orthotropic FGMs, respectively. The  $J_1^*$  and  $J_2^*$  show path-independence and convergence, while the values of  $J_1$  and  $J_2$  increase as the contours become larger. Thus, the explicit derivative

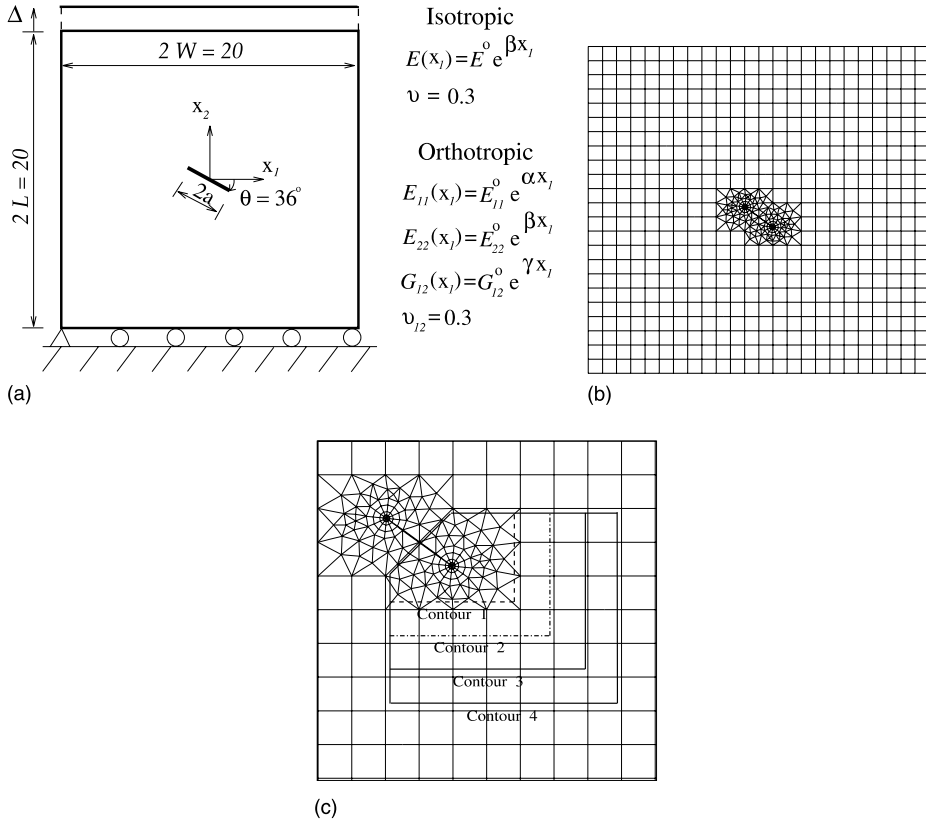


Fig. 6. Plate containing an inclined crack with angle  $\theta = 36^\circ$ : (a) geometry and BCs under fixed-grip loading; (b) complete finite element mesh; (c) contours for EDI computation of  $J_k^*$  ( $J_1^*, J_2^*$ ) and  $J_k$  ( $J_1, J_2$ ), and mesh detail using 4 rings (R4) and 12 sectors (S12) around the crack tips.

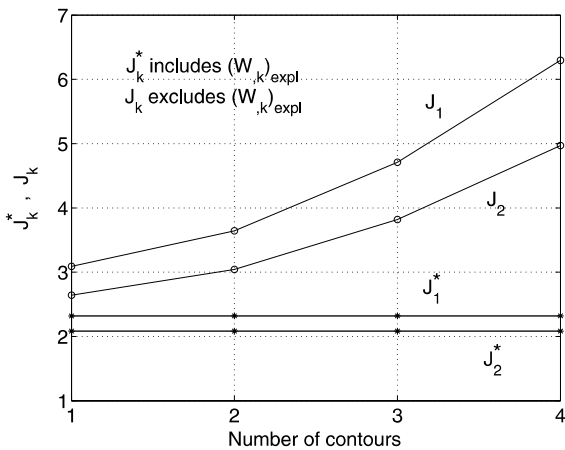


Fig. 7. Comparison of  $J_k^*$  ( $J_1^*, J_2^*$ ) and  $J_k$  ( $J_1, J_2$ ) for isotropic FGM. Note that  $J_k^*$  is path independent while  $J_k$  is path dependent.

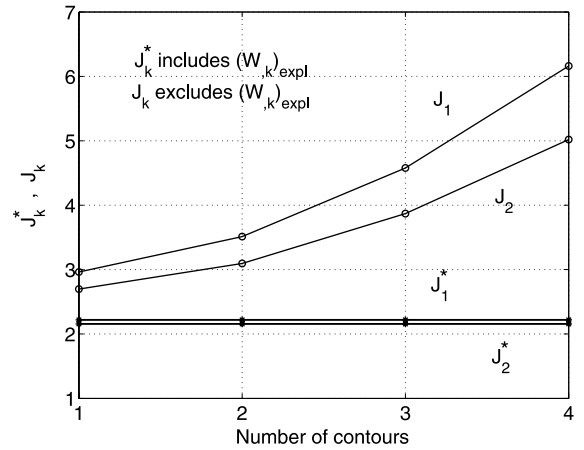


Fig. 8. Comparison of  $J_k^*$  ( $J_1^*, J_2^*$ ) and  $J_k$  ( $J_1, J_2$ ) for orthotropic FGM. Note that  $J_k^*$  is path independent while  $J_k$  is path dependent.

of the strain energy density (see Section 3) must be taken into account to ensure path-independence of the  $J^*$ -integral, especially when finite domains are considered for its evaluation.

For the orthotropic FGM case where a crack is not aligned with material directions, Newton's iteration method is used to solve for SIFs ( $K_I, K_{II}$ ) because of the nonlinear relations between  $J_k^*$  ( $k = 1, 2$ ) and ( $K_I, K_{II}$ ). The initial values for SIFs ( $K_I, K_{II}$ ) are important in the Newton's iteration method. Fig. 9 shows four possible solutions (four intersection points) for SIFs at the right crack tip, i.e. ( $K_I^{(+a)}, K_{II}^{(+a)}$ ):

$$(1.340, -1.014), \quad (1.005, -1.332), \\ (-1.340, 1.014), \quad (-1.005, 1.332)$$

Initial values for SIFs must be carefully selected for this problem because there are two sets of admissible solutions for this problem (the first two results above). If we use initial values of the SIFs obtained by the DCT, i.e. ( $K_I, K_{II}$ ) = (1.405, -0.917), the final SIFs ( $K_I, K_{II}$ ) = (1.340, -1.014) are obtained after six iterations, and are indicated in bold above (also see Fig. 9). On the other hand, other initial guesses may also lead to the correct

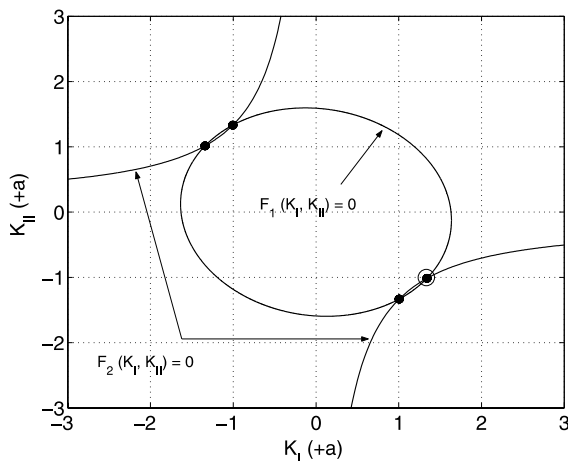


Fig. 9. SIF solution of nonlinear system of equations by Newton's iteration method considering  $(\alpha, \beta, \gamma) = (0.2, 0.25, 0.15)$  (see Fig. 6). The circle around the bullet indicates the converged solution: ( $K_I^{(+a)}, K_{II}^{(+a)} = 1.340, -1.014$ ).

solution. For instance, for the following two distinct initial guesses of ( $K_I^{(0)(+a)}, K_{II}^{(0)(+a)}$ ):

$$(1, -0.5), (1, -1)$$

the correct SIFs are obtained after six and sixteen iterations, respectively, i.e. ( $K_I^{(+a)}, K_{II}^{(+a)} = 1.340, -1.014$ ).

### 5.2. Plate with a crack parallel to material gradation

Ozturk and Erdogan (1997) have investigated the mode I crack problem for an infinite nonhomogeneous orthotropic medium. Here this problem is simulated considering  $W/a = 10$  (Fig. 10(a)). Fig. 10(a) shows a crack of length  $2a$  located in a finite two-dimensional plate under fixed grip loading and Fig. 10(b) illustrates the complete finite element mesh discretization. Fig. 10(c) shows a mesh detail with 4 rings (R4) and 16 sectors (S16) around crack tips. The applied load corresponds to  $\sigma_{22}(X_1, 10) = \varepsilon_0 E_{22}^0 e^{\beta X_1}$  along the top edge, which is equivalent to the fixed grip condition illustrated by Fig. 10(a). The displacement boundary condition is prescribed such that  $u_1 = 0$  for the left-hand corner node on the bottom edge, and  $u_2 = 0$  for all the nodes along the bottom edge.

The variations of  $E_{11}, E_{22}$ , and  $G_{12}$  are assumed to be an exponential function of  $X_1$  and proportional to one another, while the Poisson's ratio  $\nu_{12}$  is constant. The mesh has 1666 Q8, 303 T6, and 32 T6qp crack-tip singular elements with a total of 2001 elements and 5851 nodes (see Fig. 10(b)). The following data were used for the FEM analysis:

$$a/W = 0.1, \quad L/W = 1.0, \quad \varepsilon_0 = 1.0, \quad \beta a = 0.5$$

$$E_{11}(X_1) = E_{11}^0 e^{\beta X_1}, \quad E_{22}(X_1) = E_{22}^0 e^{\beta X_1},$$

$$G_{12}(X_1) = G_{12}^0 e^{\beta X_1}$$

$$\kappa_0 = 0.5$$

$$\nu = (0.1, 0.2, 0.3, 0.4, 0.5, 0.7, 0.9)$$

generalized plane stress,  $2 \times 2$  Gauss quadrature

$$(64)$$

In this case, the material nonhomogeneity is assumed such that the variations in the stiffnesses  $E_{11}, E_{22}$ , and  $G_{12}$  are *proportional* and thus

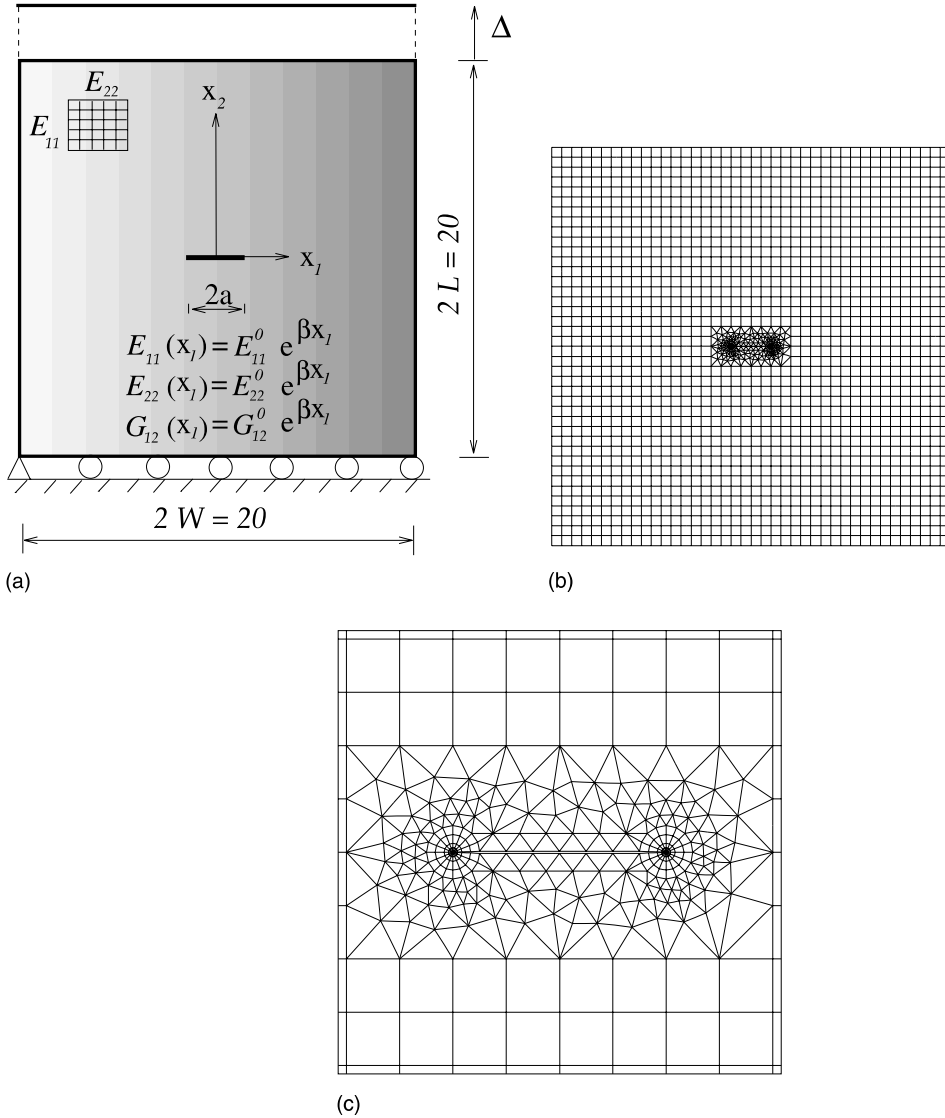


Fig. 10. Plate with a center crack parallel to the material gradation: (a) geometry and BCs under fixed-grip loading; (b) complete finite element mesh; (c) mesh detail using 4 rings (R4) and 16 sectors (S16) around crack tips.

$$\begin{aligned}
 \beta &= \frac{1}{2W} \log \left[ \frac{E_{11}(W)}{E_{11}(-W)} \right] \\
 &= \frac{1}{2W} \log \left[ \frac{E_{22}(W)}{E_{22}(-W)} \right] \\
 &= \frac{1}{2W} \log \left[ \frac{G_{12}(W)}{G_{12}(-W)} \right]
 \end{aligned} \tag{65}$$

Notice that  $\beta$  has units  $[\text{length}]^{-1}$ .

Table 1 compares the normalized SIFs using the  $J_k^*$ -integral in an orthotropic plate under fixed-grip loading with those reported by Ozturk and Erdogan (1997). The FEM results obtained by means of the  $J_k^*$ -integral agree with the SIFs obtained by Ozturk and Erdogan (1997) to within 2%. Notice that the effective Poisson's ratio  $\nu = \sqrt{\nu_{12}\nu_{21}}$  has a negligible effect on the SIFs for the mode I crack problem.

Table 1

Normalized SIFs in an inhomogeneous orthotropic plate under fixed grip loading for various Poisson’s ratios—mode I ( $\beta a = 0.5, \kappa_0 = 0.5, K_0 = \epsilon_0 E^0 \sqrt{\pi a}; \bar{E}^0 = E^0/\delta^2; E^0 = \sqrt{E_{11}^0 E_{22}^0}$ )

v	$J_k^*$ integral		Ozturk and Erdogan (1997)	
	$K_I(+a)/K_0$	$K_I(-a)/K_0$	$K_I(+a)/K_0$	$K_I(-a)/K_0$
0.1	1.4451	0.6776	1.4183	0.6647
0.2	1.4488	0.6802	1.4233	0.6676
0.3	1.4522	0.6822	1.4280	0.6704
0.4	1.4559	0.6843	1.4325	0.6730
0.5	1.4593	0.6864	1.4368	0.6755
0.7	1.4655	0.6902	1.4449	0.6802
0.9	1.4718	0.6939	1.4524	0.6846

5.3. Plate with a crack perpendicular to material gradation

Ozturk and Erdogan (1999) have investigated the mixed-mode crack problem for an infinite nonhomogeneous orthotropic medium. Fig. 11(a) and (b) show a crack of length  $2a$  located in a finite two-dimensional plate under remote uniform tension loading for two different boundary conditions. These boundary conditions are prescribed such that, for Fig. 11(a),  $u_1 = 0$  along the left and right edges and, in addition,  $u_2 = 0$  for the node in the middle of the left edge, while for Fig. 11(b),  $u_1 = 0$  for the left corner node of the bottom edge and  $u_2 = 0$  along the bottom edge. The finite element mesh configurations are the same as in the previous

example (see Fig. 10(b) and (c)). The applied load corresponds to  $\sigma_{22}(X_1, \pm L) = \pm\sigma = \pm 1.0$  for the BC in Fig. 11(a), and  $\sigma_{22}(X_1, L) = \sigma = 1.0$  for the BC in Fig. 11(b).

The variations of  $E_{11}$ ,  $E_{22}$ , and  $G_{12}$  are exponential functions of  $X_2$  and are proportional, while the Poisson’s ratio  $\nu_{12}$  is constant. The following data were used for the FEM analysis:

$$a/W = 1/9, 1/10, 1/11, 1/13, 1/15, \quad L/W = 1.0,$$

$$E_{11}(X_2) = E_{11}^0 e^{\beta X_2}, \quad E_{22}(X_2) = E_{22}^0 e^{\beta X_2},$$

$$G_{12}(X_2) = G_{12}^0 e^{\beta X_2},$$

dimensionless nonhomogeneity parameter:

$$\beta a = (0.0 \text{ to } 0.5),$$

$$\delta^4 = E_{11}/E_{22} = (0.25, 0.5, 1.0, 3.0, 10.0),$$

$$\kappa_0 = (-0.25, 0.0, 0.5, 1.0, 2.0, 5.0), \quad \nu = 0.30,$$

generalized plane stress,  $2 \times 2$  Gauss quadrature (66)

Similarly to the previous example, the material nonhomogeneity is assumed such that the variations in the stiffnesses  $E_{11}$ ,  $E_{22}$ , and  $G_{12}$  are *proportional* and thus

$$\begin{aligned} \beta &= \frac{1}{2L} \log \left[ \frac{E_{11}(L)}{E_{11}(-L)} \right] = \frac{1}{2L} \log \left[ \frac{E_{22}(L)}{E_{22}(-L)} \right] \\ &= \frac{1}{2L} \log \left[ \frac{G_{12}(L)}{G_{12}(-L)} \right] \end{aligned} \quad (67)$$

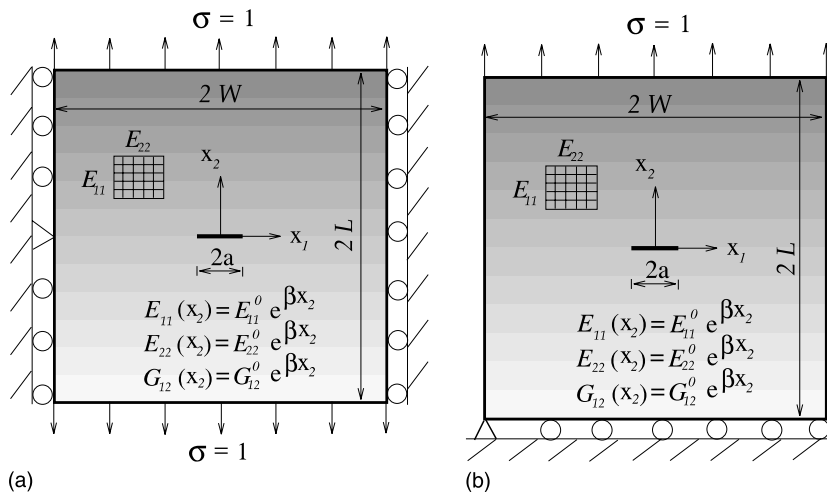


Fig. 11. Plate with a center crack perpendicular to the material gradation: (a) first set of BCs; (b) second set of BCs.

As before,  $\beta$  has units  $[\text{length}]^{-1}$ . Therefore  $1/\beta$  is the single length scale of nonhomogeneity for this specific problem.

Figs. 12 and 13 show the FEM results for normalized strain energy release rates with varying  $\delta^4$  and fixed  $\beta a = 0.5$  using various plate size and considering the two BCs of Fig. 11(a) and (b), respectively. The normalizing strain energy release rate  $\mathcal{G}_0 = \pi\sigma^2 a/E^0$  corresponds to a homogeneous isotropic medium ( $\beta a = 0, \kappa_0 = 1, \delta^4 = 1$ ). For the BC of Fig. 11(a), Fig. 12 shows that there is no size

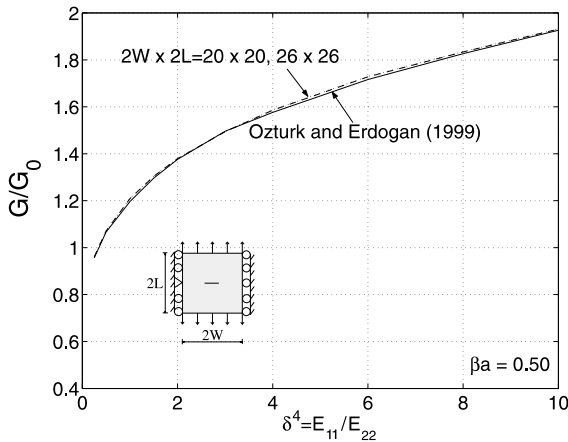


Fig. 12. Normalized strain energy release rate versus  $\delta^4$  for  $\beta a = 0.5$ . There is no size-effect for this case (first set of BCs).

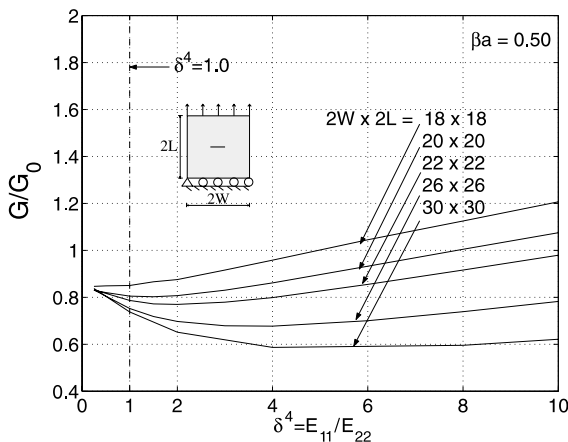


Fig. 13. Size-effect on normalized strain energy release rate versus  $\delta^4$  for  $\beta a = 0.5$ . Notice the pronounced size-effect for this case (second set of BCs).

effect on  $\mathcal{G}/\mathcal{G}_0$ , which matches well the results by Ozturk and Erdogan (1999) for an infinite medium; while for the BC of Fig. 11(b), there is a significant size-effect on  $\mathcal{G}/\mathcal{G}_0$ , as illustrated by Fig. 13. As the plate size changes, the solution also changes. Notice that the effect of plate size on  $\mathcal{G}/\mathcal{G}_0$  strongly depends on far-field boundary conditions in FGMs, however, such phenomenon is not observed in homogeneous materials (cf. Paulino et al., 1993).

The effect of boundary conditions and material gradation on  $\mathcal{G}/\mathcal{G}_0$  are investigated by fixing plate size  $2W \times 2L = 20 \times 20$ . Fig. 14 shows plots of normalized strain energy release rates in a non-homogeneous orthotropic plate under uniform tension for two different boundary conditions for a fixed stiffness ratio  $\delta^4 = 10$  and constant Poisson's ratio  $\nu = 0.3$  with varying material nonhomogeneity  $\beta a$  and  $\kappa_0$ . It is clearly observed that the boundary conditions and the Poisson's ratio have much influence on the strain energy release rates and SIFs. The boundary condition of Fig. 11(a) prohibits the Poisson's effect of contraction in the  $X_1$  direction. When using this BC (see Fig. 11(a)), the FEM results agree with the normalized strain energy release rates ( $\mathcal{G}/\mathcal{G}_0$ ) obtained by Ozturk and Erdogan (1999), which are monotonically in-

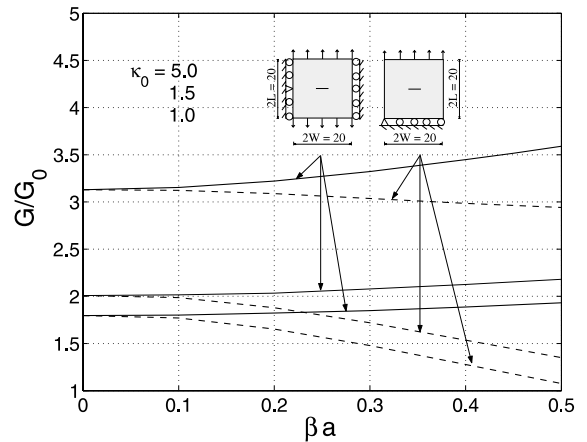


Fig. 14. Normalized strain energy release rate versus the non-homogeneity parameter  $\beta a$  and the shear parameter  $\kappa_0$  considering uniformly applied tension ( $\sigma_{22}(X_1, \pm L) = \pm\sigma$  for the first set of BCs and  $\sigma_{22}(X_1, L) = \sigma$  for the second set of BCs) and  $\delta^4 = 10.0, \nu = 0.3, \mathcal{G}_0 = \pi\sigma^2 a/E^0$ .

creasing functions of  $\kappa_0$  and  $\beta a$ . However, for the other BC (see Fig. 11(b)), the results (dashed lines in Fig. 14) differ significantly from the previous ones (solid lines in Fig. 14). Notice that, for the case illustrated by Fig. 11(b), although  $\mathcal{G}/\mathcal{G}_0$  is still an increasing function of  $\kappa_0$ , it is a decreasing function of  $\beta a$ .

Figs. 15 and 16 give the FEM results for a fixed  $\kappa_0 = 1$  with varying  $\delta^4$  and  $\beta a$  for the two BCs of Fig. 11(a) and (b), respectively. For the BC of Fig. 11(a), Fig. 15 shows that  $\mathcal{G}/\mathcal{G}_0$  is an increasing function of  $\delta^4$ , which agrees well with the results by Ozturk and Erdogan (1999). Moreover,  $\mathcal{G}/\mathcal{G}_0$  is a monotonically increasing function of  $\beta a$ . However, for the BC of Fig. 11(b), the overall behavior is quite different as shown by Fig. 16. Note that  $\mathcal{G}/\mathcal{G}_0$  is a monotonically increasing function of  $\beta a$  for  $\delta^4 = 0.25$  and a monotonically decreasing function of  $\beta a$  for  $\delta^4 = 10$ .

Figs. 17 and 18 show the FEM results with varying  $\beta a$  and  $\delta^4$  considering the two BCs of Fig. 11(a) and (b), respectively. For the BC of Fig. 11(a), Fig. 17 shows that  $\mathcal{G}/\mathcal{G}_0$  is an increasing function of  $\beta a$ , which matches well the results by Ozturk and Erdogan (1999); while for the BC of Fig. 11(b),  $\mathcal{G}/\mathcal{G}_0$  loses such trends for  $\beta a$  as illustrated by Fig. 18. Fig. 19 shows an enlargement for the transition region  $\delta^4 = (0.25-2.0)$ , observed in

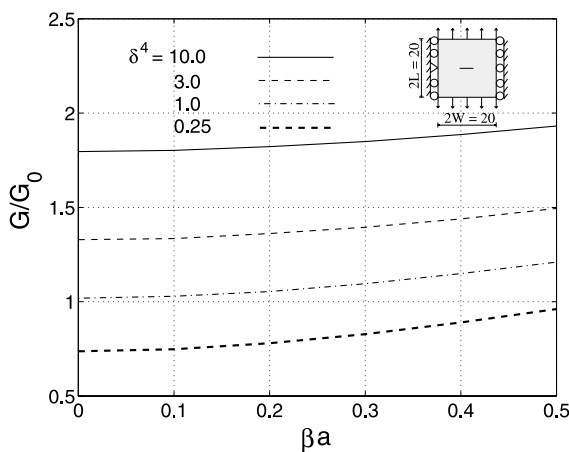


Fig. 15. Normalized strain energy release rate with the non-homogeneity parameter  $\beta a$  and the stiffness parameter  $\delta^4$  considering uniform tension (first set of BCs), and  $\sigma_{22}(X_1, \pm L) = \pm\sigma$ ,  $\kappa_0 = 1$ ,  $\nu = 0.3$ ,  $\mathcal{G}_0 = \pi\sigma^2 a/E^0$ .

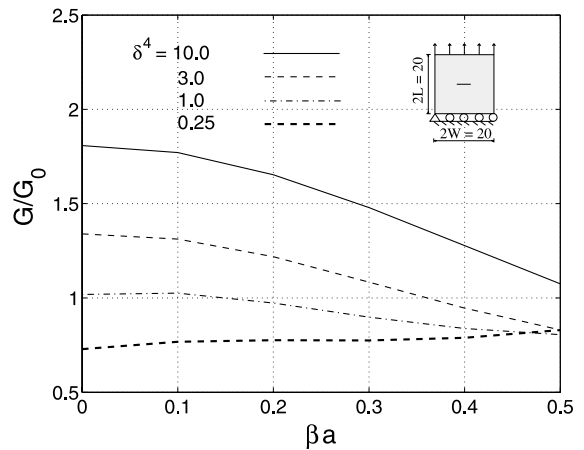


Fig. 16. Normalized strain energy release rate with the non-homogeneity parameter  $\beta a$  and the stiffness parameter  $\delta^4$  considering uniform tension (second set of BCs), and  $\sigma_{22}(X_1, L) = \sigma$ ,  $\kappa_0 = 1$ ,  $\nu = 0.3$ ,  $\mathcal{G}_0 = \pi\sigma^2 a/E^0$ .

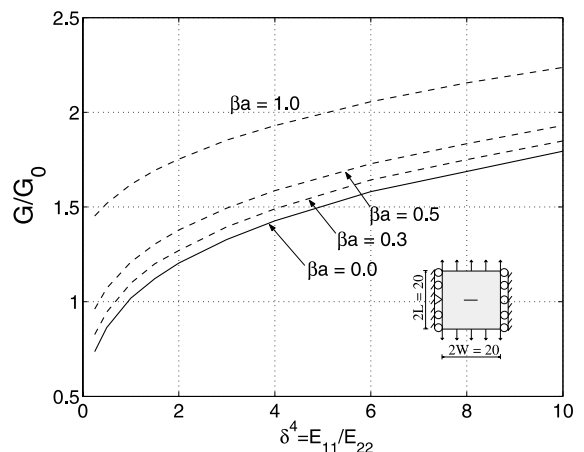


Fig. 17. Normalized strain energy release rate with the stiffness parameter  $\delta^4$  and the nonhomogeneity parameter  $\beta a$  considering uniform tension (first set of BCs), and  $\sigma_{22}(X_1, \pm L) = \pm\sigma$ ,  $\kappa_0 = 1$ ,  $\nu = 0.3$ ,  $\mathcal{G}_0 = \pi\sigma^2 a/E^0$ .

Fig. 18. The region around  $\delta^4 = 1$  is of special interest because of the change of the stiffness ratio  $E_{11}/E_{22}$  (from  $E_{11} < E_{22}$  to  $E_{11} > E_{22}$ ). Notice that, for this particular case of a  $20 \times 20$  plate with a center crack, the curves for the nonhomogeneous materials meet near  $\delta^4 = 0.5$ . However, this location changes as the plate size changes (size-effect). Fig. 20 shows a comparison of the FEM results

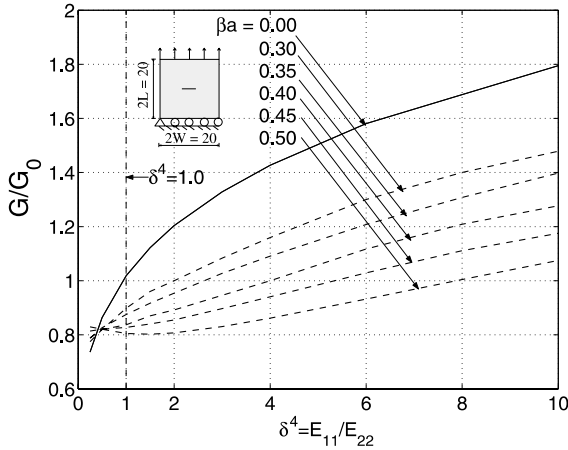


Fig. 18. Normalized strain energy release rate with the stiffness parameter  $\delta^4$  and the nonhomogeneity parameter  $\beta a$  considering uniform tension (second set of BCs), and  $\sigma_{22}(X_1, L) = \sigma$ ,  $\kappa_0 = 1$ ,  $\nu = 0.3$ ,  $\mathcal{G}_0 = \pi\sigma^2 a/E^0$ .

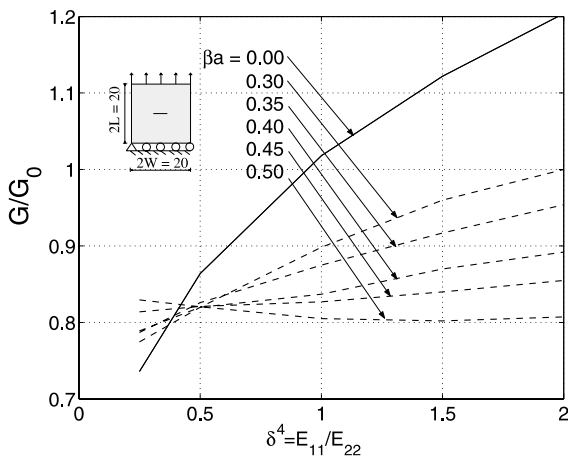


Fig. 19. Zoom of Fig. 18 for the range of  $\delta^4 = (0.25\text{--}2.0)$ .

obtained by the present method (using the path-independent  $J_k^*$ -integral) with those obtained by the modified crack closure (MCC) method (Kim and Paulino, 2002c). Notice that there is relatively good agreement between the two methods.

Figs. 21 and 22 show the variation of  $\mathcal{G}/\mathcal{G}_0$  with  $\beta a$  and  $\kappa_0$  for a fixed  $\delta^4 = 9$  considering the two BCs of Fig. 11(a) and (b), respectively. For the BC of Fig. 11(a), Fig. 21 shows that  $\mathcal{G}/\mathcal{G}_0$  is an increasing function of  $\beta a$  and  $\kappa_0$  for  $\delta^4 = 9$ , which agrees with the results by Ozturk and Erdogan

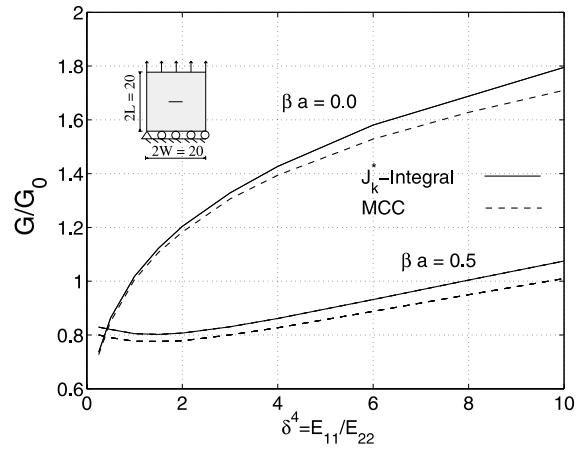


Fig. 20. Comparison of the FEM results obtained by the present method and the MCC method (Kim and Paulino, 2002c) for normalized strain energy release rate versus the stiffness parameter  $\delta^4$  and the nonhomogeneity parameter  $\beta a$  considering uniform tension (second set of BCs), and  $\sigma_{22}(X_1, L) = \sigma$ ,  $\kappa_0 = 1$ ,  $\nu = 0.3$ ,  $\mathcal{G}_0 = \pi\sigma^2 a/E^0$ .

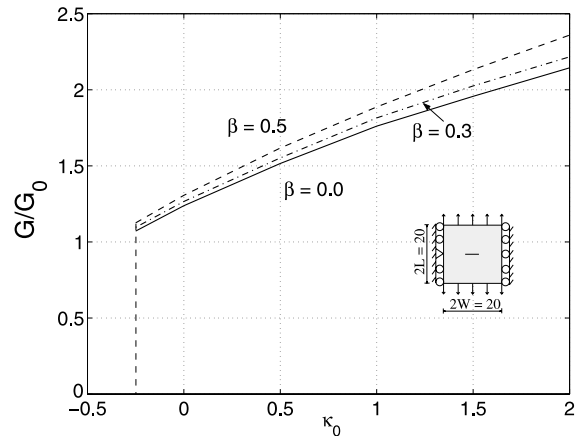


Fig. 21. Normalized strain energy release rate with the shear parameter  $\kappa_0$  and the nonhomogeneity parameter  $\beta a$  considering uniform tension (first set of BCs), and  $\sigma_{22}(X_1, \pm L) = \pm\sigma$ ,  $\delta^4 = 9$ ,  $\nu = 0.3$ ,  $\mathcal{G}_0 = \pi\sigma^2 a/E^0$ .

(1999). However, for the BC of Fig. 11(b), Fig. 22 shows that  $\mathcal{G}/\mathcal{G}_0$  is a decreasing function of  $\beta a$  and  $\kappa_0$  for  $\delta^4 = 9$ . Notice that the FEM results are obtained for  $\kappa_0 \geq -0.25$ . To ensure that the expression  $E/(2G_{12}) = \kappa_0 + \nu$  in Eq. (60) is satisfied for the range of material properties considered here, the shear parameter  $\kappa_0$  should be greater than  $-0.3$ .

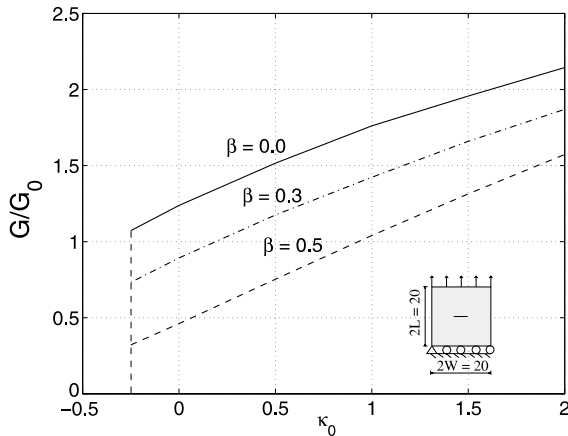


Fig. 22. Normalized strain energy release rate with the shear parameter  $\kappa_0$  and the nonhomogeneity parameter  $\beta a$  considering uniform tension (second set of BCs), and  $\sigma_{22}(X_1, L) = \sigma$ ,  $\delta^d = 9$ ,  $\nu = 0.3$ ,  $\mathcal{G}_0 = \pi\sigma^2 a/E^0$ .

In summary, the BCs, plate size, material gradation, and orthotropy may have a significant influence on fracture behavior. Due to the intrinsic length scales of material nonhomogeneity ( $1/\beta$  in Eq. (67), which has units of [length]), there exists an interplay between the geometrical length scale of the boundary value problem and the length scale of material gradation (cf. Figs. 12 and 13).

5.4. Poisson’s ratio effect

As pointed out in Section 5.2, where a mode I crack is investigated (crack parallel to the material gradation—see Fig. 10(a)), the Poisson’s ratio has

a negligible effect on the SIFs, as evidenced by the results shown in Table 1. However, for the mixed-mode crack problem (e.g. crack perpendicular to the material gradation—see Fig. 11(b)), the Poisson’s ratio has much influence on the SIFs. This point is shown by considering the results of Table 2 for the plate of Fig. 11(b) with  $E_{11}$ ,  $E_{22}$ , and  $G_{12}$  exponential functions of  $X_2$ , which is under uniformly applied remote tension load  $\sigma_{22}(X_1, 10) = 1.0$ , and by comparing the results with those of Table 1.

6. Conclusions and extensions

This paper presents the path-independent  $J_k^*$ -integral formulation, in conjunction with a corresponding general purpose FEM, for mixed-mode crack problems considering cracks arbitrarily oriented with respect to the principal axes of orthotropy in linearly elastic orthotropic FGMs. The path-independent  $J_k^*$ -integral formulation, previously developed for isotropic FGMs, is extended to orthotropic FGMs. The  $J_k^*$ -integral includes the explicit derivative of the strain energy density and exhibits path-independence for mixed-mode problems. The numerical results show good agreement with the semi-analytical solutions by Ozturk and Erdogan (1999), which are valid for an infinite orthotropic nonhomogeneous medium having proportional stiffness ( $E_{11}, E_{22}, G_{12}$ ) and constant Poisson’s ratio with a single crack along a principal orthotropy direction. In general, such solutions provide higher accuracy than numerical solutions, however, the present FEM implementation, using the  $J_k^*$ -integral formulation, does not have any of these limitations, and is valid for any material variation, any BCs, and multiple cracks with arbitrary orientation in finite bodies.

Plate size, material property gradation (isotropy or orthotropy), and BCs play a significant role in fracture behavior of FGMs. For a given plate size, the effect of material gradation is characterized by the length scale of material gradation, which interplays with the geometrical length scale. Thus, in general, the ratio of crack size to the dimensions of a plate ( $a/W$ ) does not lead to a converged solution when approximating an infinite domain with a

Table 2  
Normalized SIFs in an inhomogeneous orthotropic plate under remote constant loading for various Poisson’s ratios—mixed-mode ( $\beta a = 0.5, \kappa_0 = 0.5$ )

$\nu$	$J_k^*$ -integral	
	$K_I$	$K_{II}$
0.1	1.6140	0.1992
0.2	1.4162	0.1878
0.3	1.2404	0.1773
0.4	1.0836	0.1674
0.5	0.9428	0.1577
0.7	0.7010	0.1378
0.9	0.5014	0.1018

finite domain for boundary value problems in FGMs. However, this behavior is not observed in homogeneous materials. Moreover, the numerical results obtained indicate that the Poisson's ratio has a significant influence on SIFs and mode-mixity for mixed-mode crack problems with prescribed boundary conditions, while it has a negligible effect for pure mode I problems.

The potential extensions of this work include development of fracture criteria and simulation crack propagation for orthotropic FGMs. The computational simulations need to be validated by means of carefully executed experiments. These topics are currently under investigation by the authors.

### Acknowledgements

This work was supported by the National Science Foundation (NSF) under grant CMS-0115954 (Mechanics & Materials Program). Additional support for this work was provided by the NASA-Ames "Engineering for Complex Systems Program", and the NASA-Ames Chief Engineer (Dr. Tina Panontin) through grant NAG 2-1424.

### References

- Anlas, G., Santare, M.H., Lambros, J., 2000. Numerical calculation of stress intensity factors in functionally graded materials. *International Journal of Fracture* 104, 131–143.
- Bao, G., Cai, H., 1997. Delamination cracking in functionally graded coating/metal substrate systems. *Acta Mechanica* 45 (3), 1055–1066.
- Bao, G., Wang, L., 1995. Multiple cracking in functionally graded ceramic/metal coatings. *International Journal of Solids and Structures* 32 (19), 2853–2871.
- Chen, J., Wu, L., Du, S., 2000. A modified  $J$  integral for functionally graded materials. *Mechanics Research Communications* 27 (3), 301–306.
- Choules, B.D., Kokini, K., 1993. In: Kokini, K. (Ed.), *Ceramic Coatings*, ASME MD, 44, pp. 73–86.
- Christensen, R.M., 1979. *Mechanics of Composite Materials*. John Wiley & Sons, Inc., New York.
- Delale, F., Erdogan, F., 1983. The crack problem for a nonhomogeneous plane. *Journal of Applied Mechanics* 50, 609–614.
- Desplat, J.L., 1996. Recent development on oxygenated thermionic energy converter—Overview. In: *Proceedings of the Fourth International Symposium on Functionally Graded Materials*, Tsukuba City, Japan.
- Dolbow, J., Gosz, M., 2002. On the computation of mixed-mode stress intensity factors in functionally graded materials. *International Journal of Solids and Structures* 39 (9), 2557–2574.
- Eischen, J.W., 1987. Fracture of nonhomogeneous materials. *International Journal of Fracture* 34, 3–22.
- Erdogan, F., Wu, B.H., 1993. Analysis of FGM specimen for fracture toughness testing. In: *Ceramic Transactions*, 34. The American Ceramic Society, Westerville, OH, pp. 39–46.
- Erdogan, F., Wu, B.H., 1996. Crack problems in FGM layers under thermal stresses. *Journal of Thermal Stresses* 19, 237–265.
- Gu, P., Asaro, R.J., 1997. Cracks in functionally graded materials. *International Journal of Solids and Structures* 34 (1), 1–17.
- Gu, P., Dao, M., Asaro, R.J., 1999. A simplified method for calculating the crack-tip field of functionally graded materials using the domain integral. *ASME Journal of Applied Mechanics* 66 (1), 101–108.
- Hirai, T., 1993. Functionally gradient materials and nanocomposites. In: Holt, J.B., Koizumi, M., Hirai, T., Munir, Z.A. (Eds.), *Proceedings of the Second International Symposium on Functionally Gradient Materials*, Ceramic Transactions, 34. The American Ceramic Society, Westerville, OH, pp. 11–20.
- Hirano, T., Whitlow, L.W., Miyajima, M., 1993. Numerical analysis of efficiency improvement in functionally gradient thermoelectric materials. In: Holt, J.B., Koizumi, M., Hirai, T., Munir, Z.A. (Eds.), *Proceedings of the Second International Symposium on Functionally Gradient Materials*, Ceramic Transactions, 34. The American Ceramic Society, Westerville, OH, pp. 23–30.
- Honein, T., Herrmann, G., 1997. Conservation laws in nonhomogeneous plane elastostatics. *Journal of the Mechanics and Physics of Solids* 45, 789–805.
- Igari, T., Notomi, A., Tsunoda, H., Hida, K., Kotoh, T., Kunishima, S., 1990. Material properties of functionally gradient material for fast breeder reactor. In: Yamanouchi, M., Koizumi, M., Hirai, T., Shiota, I. (Eds.), *Proceedings of the First International Symposium on Functionally Gradient Materials*, Sendai, Japan, pp. 209–214.
- Jin, Z.-H., Batra, R.C., 1996. Stress intensity relaxation at the tip of an edge crack in a functionally graded material subjected to a thermal shock. *Journal of Thermal Stresses* 19, 317–339.
- Jin, Z.-H., Noda, N., 1993. An internal crack parallel to the boundary of a nonhomogeneous half plane under thermal loading. *International Journal of Engineering Science* 31, 793–806.
- Jin, Z.-H., Paulino, G.H., 2001. Transient thermal stress analysis of an edge crack in a functionally graded material. *International Journal of Fracture* 107 (1), 73–98.

- Kaysser, W.A., Ilshner, B., 1995. FGM research activities in Europe. *MRS Bulletin* 20 (1), 22–26.
- Kim, J.-H., Paulino, G.H., 2002a. Finite element evaluation of mixed mode stress intensity factors in functionally graded materials. *International Journal for Numerical Methods in Engineering* 53 (8), 1903–1935.
- Kim, J.-H., Paulino, G.H., 2002b. Isoparametric graded finite elements for nonhomogeneous isotropic and orthotropic materials. *ASME Journal of Applied Mechanics* 69 (4), 502–514.
- Kim, J.-H., Paulino, G.H., 2002c. Mixed-mode fracture of orthotropic functionally graded materials using finite elements and the modified crack closure method. *Engineering Fracture Mechanics* 69 (14–16), 1557–1586.
- Kim, J.-H., Paulino, G.H., submitted for publication. An accurate scheme for mixed-mode fracture analysis of functionally graded materials using the interaction integral and micromechanics models. *International Journal for Numerical Methods in Engineering*.
- Koike, Y., 1992. Graded-index and single mode polymer optical fibers. In: Chiang, L.Y., Garito, A.G., Sandman, D.J. (Eds.), *Electrical, Optical, and Magnetic Properties of Organic Solid State Materials*, 247. Materials Research Society Proceedings, Pittsburgh, PA, p. 817.
- Koizumi, M., 1993. The concept of FGM. In: Holt, J.B., Koizumi, M., Hirai, T., Munir, Z.A. (Eds.), *Proceedings of the Second International Symposium on Functionally Graded Materials*, Ceramic Transactions, 34. The American Ceramic Society, Westerville, OH, pp. 3–10.
- Krenk, S., 1979. On the elastic constants of plane orthotropic elasticity. *Journal of Composite Materials* 13, 108–116.
- Kurihara, K., Sakaki, K., Kawarada, M., 1990. Adhesion improvement of diamond films. In: Yamanouchi, M., Koizumi, M., Hirai, T., Shiota, I. (Eds.), *Proceedings of the First International Symposium on Functionally Graded Materials*, Tokyo, Japan, pp. 65–69.
- Lee, Y.D., Erdogan, F., 1995. Residual/thermal stresses in FGM and laminated thermal barrier coatings. *International Journal of Fracture* 69, 145–165.
- Lekhnitskii, S.G., 1968. *Anisotropic Plates*. Gordon and Breach, New York.
- Ma, H., Chen, Y.H., 1996. The explicit formulation for  $J_k$ -vector in both isotropic and anisotropic cases. *International Journal of Fracture* 75, R25–R28.
- Marur, P.R., Tippur, H.V., 2000. Numerical analysis of crack-tip fields in functionally graded materials with a crack normal to the elastic gradient. *International Journal of Solids and Structures* 37, 5353–5370.
- Miyamoto, Y., Kaysser, W.A., Rabin, B.H., Kawasaki, A., Ford, R.G., 1999. *Functionally Graded Materials: Design, Processing, and Applications*. Kluwer Academic Publishers, Dordrecht.
- Noda, N., Jin, Z.-H., 1993. Thermal stress intensity factors for a crack in a strip of a functionally graded materials. *International Journal of Solids and Structures* 30, 1039–1056.
- Obata, M., Nemat-Nasser, S., Goto, Y., 1989. Branched cracks in anisotropic elastic solids. *ASME Journal of Applied Mechanics* 56, 858–864.
- Oonishi, H., Noda, T., Ito, S., Kohda, A., Yamamoto, H., Tsuji, E., 1994. Effect of hydroxyapatite coating on bone growth into porous titanium alloy implants under loaded conditions. *Journal of Applied Biomaterials* 5 (1), 23–27.
- Osaka, T., Matsubara, H., Homma, T., Mitamura, S., Noda, K., 1990. Microstructural study of electroless-plated CoNi-ReP/NiMoP double-layered media for perpendicular magnetic recording. *Japanese Journal of Applied Physics* 29 (10), 1939–1943.
- Ozturk, M., Erdogan, F., 1997. Mode I crack problem in an inhomogeneous orthotropic medium. *International Journal of Engineering Science* 35 (9), 869–883.
- Ozturk, M., Erdogan, F., 1999. The mixed mode crack problem in an inhomogeneous orthotropic medium. *International Journal of Fracture* 98, 243–261.
- Paulino, G.H., Kim, J.-H., submitted for publication. The weak patch test for nonhomogeneous materials modeled with graded finite elements.
- Paulino, G.H., Saif, M.T.A., Mukherjee, S., 1993. A finite elastic body with a curved crack loaded in anti-plane shear. *International Journal of Solids and Structures* 30 (8), 1015–1037.
- Paulino, G.H., Jin, Z.-H., Dodds Jr., R.H., 2003. Failure of functionally graded materials. In: Karihaloo, B. et al. (Eds.), *Comprehensive Structural Integrity*, Vol. 2. Elsevier, Amsterdam, Ch. 13.
- Raju, I.S., 1990. An equivalent domain integral method in the two-dimensional analysis of mixed mode crack problems. *Engineering Fracture Mechanics* 37 (4), 707–725.
- Rao, B.N., Rahman, S., in press. Mesh-free analysis of cracks in isotropic functionally graded materials. *Engineering Fracture Mechanics*.
- Reiter, T., Dvorak, G.J., Tvergaard, V., 1997. Micromechanical models for graded composite materials. *Journal of the Mechanics and Physics in Solids* 45, 1281–1302.
- Rice, J.R., 1968. Path-independent integral and the approximate analysis of strain concentration by notches and cracks. *ASME Journal of Applied Mechanics* 35, 379–386.
- Sampath, S., Herman, H., Shimoda, N., Saito, T., 1995. Thermal spray processing of FGMs. *MRS Bulletin* 20 (1), 27–31.
- Sih, G.C., Paris, P.C., Irwin, G.R., 1965. On cracks in rectilinearly anisotropic bodies. *International Journal of Fracture Mechanics* 1, 189–203.
- Suresh, S., Mortensen, A., 1998. *Fundamentals of Functionally Graded Materials*. IOM Communications Ltd, London.
- Tani, J., Liu, G.R., 1993. Surface waves in functionally gradient piezoelectric plates. *JSME International Journal Series A (Mechanics and Material Engineering)* 36 (2), 152–155.
- Watanabe, Y., Nakamura, Y., Fukui, Y., Nakanishi, K., 1993. A magnetic-functionally graded material manufactured with deformation-induced martensitic transformation. *Journal of Materials Science Letters* 12 (5), 326–328.

- Watari, F., Yokoyama, A., Saso, F., Uo, M., Ohkawa, S., Kawasaki, T., 1996. EPMA elemental mapping of functionally graded dental implant in biocompatibility test. In: Proceedings of the Fourth International Symposium on Functionally Graded Materials, Tsukuba City, Japan.
- Wawrzynek, P.A., 1987. Interactive finite element analysis of fracture processes: an integrated approach. M.S. Thesis, Cornell University.
- Wawrzynek, P.A., Ingraffea, A.R., 1991. Discrete modeling of crack propagation: theoretical aspects and implementation issues in two and three dimensions. Report 91-5, School of Civil Engineering and Environmental Engineering, Cornell University.
- Zuiker, J.R., 1995. Functionally graded materials: choice of micromechanics model and limitations in property variation. *Composites Engineering* 5 (7), 807–819.